Korean J. Chem. Eng., 40(8), 1928-1953 (2023)
DOI: 10.1007/s11814-023-1450-y

pISSN: 0256-1115
eISSN: 1975-7220

Equilibrium, kinetic and thermodynamic studies of the adsorption of trypan blue dye by *Pseudomonas* sp. strain MM02 inactivated biomass

Abdussamad Abubakar[*,], Motharasan Manogaran[*,***], Nur Adeela Yasid[*], Ahmad Razi Othman[****], and Mohd Yunus Abd Shukor[*,†]**

*Department of Biochemistry, Faculty of Biotechnology and Biomolecular Sciences Universiti Putra Malaysia, 43400 UPM Serdang, Selangor, D. E, Malaysia
**Department of Microbiology, Faculty of Science, Bauchi State University Gadau, P. M. B. 65, Nigeria
***Malaysia Genome and Vaccine Institute (MGVI) National Institute of Biotechnolgy Malaysia (NIBM) Jalan Bangi, 43000 Kajang, Selangor, Malaysia
****Department of Chemical Engineering, Faculty of Engineering and Built Environment, Universit Kebangsaan Malaysia, 43600 UKM Bangi, Selangor, D.E, Malaysia
(*Received 9 July 2022 • Revised 15 December 2022 • Accepted 31 January 2023*)

Abstract−More concerning about dye pollution is that it is being worsened by a lack of adequate treatment. This study optimized the adsorption of Trypan Blue (TB) dye in an aqueous solution using screened bacterial biomass. Among twelve different bacterial isolates screened against TB dye, *Pseudomonas* sp. strain MM02 showed a high adsorption percentage of 36.5%. The adsorption process was enhanced using one-factor-at-a-time (OFAT) and response surface methodology (RSM) optimization. An adsorption of 59% was achieved through OFAT optimization (TB dye concentration 15 ppm, contact time 20 min, pH 6.5, agitation speed 150 rpm, adsorbent amount 1.10 g and temperature 30 °C), while statistical optimization using RSM resulted in a further increased adsorption of the dye to 61.51% (TB dye concentration 22.27 ppm, adsorbent size 0.32 g, and temperature 34.27 °C). The results of this investigation demonstrated that OFAT and RSM optimization were effective and that they were also appropriate strategies for optimizing the adsorption of TB dye by *Pseudomonas* sp. strain MM02. Thus, it is possible to achieve the necessary water quality while saving money by using the strain MM02 of *Pseudomonas* sp. MM02 in a water treatment facility. Changes in free energy of adsorption (ΔG^o), enthalpy (ΔH^o) and entropy (ΔS^o) as well as the activation energy (Ea) were determined. ΔH^o, ΔS^o and Ea with pH control were −26.5, −230 and 43.5 kJ/mol. The result showed that bacterial cellulose could be employed as an effective sorbent for the removal of direct dye from an aqueous solution and the values of ΔH^o, ΔG^o and Ea indicate that the adsorption of direct dye onto bacterial cellulose was a physisorption process: ΔG^o and ΔH^o.

Keywords: Adsorption, Trypan Blue, *Pseudomonas* sp. Strain MM02, One-factor-at-a-time, Response Surface Methodology, Kinetics, Isotherms And Thermodynamics

INTRODUCTION

As a result of dye pollution, water contamination has been recognized as a severe issue worldwide [1-3]. Dye pollution sources include textile, food, paper-making, cosmetic industries, and medical and research centers [4-7]. Dye pollution is still increasing in many developing countries with less strict regulations on the manufacturing and use of dyes. Some examples of these countries include Malaysia, India, Pakistan, and Bangladesh [8,9]. In Malaysia, the Juru riverine area has been documented to have high-level contamination of dye pollution [9,10]. Effluents from dye-utilizing industries are usually released directly into the water bodies, becoming a significant wastewater treatment concern [11,12]. In addition, many of the dyes and their byproducts have been documented to be mutagenic and carcinogenic, as well as xenobiotic and recalcitrant pollutants [12-14]. Therefore, even in small amounts dyes have been reported to pose a serious threat to human health and the environment, including the aquatic ecosystem [11]. Other challenges of dye pollution include increasing the chemical oxygen demand (COD) and biological oxygen demand (BOD), compromising the photosynthesis and the aesthetic quality of the water bodies [15,16].

Dyes are highly soluble in water and because of that some of the conventional wastewater treatment processes do not effectively clean the contaminants [17]. Traditionally, the effective treatment of dye effluents involves combining biological, chemical, and physical processes, such as precipitation, coagulation, ion exchange, reverse osmosis, flocculation, membrane filtration, photoelectrochemistry, and incineration [18]. Nevertheless, because of the excessive usage of chemicals in some cases, the implementation of these processes may significantly generate secondary metabolites or sludge [19,20]. Furthermore, these conventional methods have also been shown to have some disadvantages: high production and maintenance costs, low dye removal efficiency, and possible generation of toxic by-products [21].

In the alternative, biosorption has been researched and proclaimed a promising technology in providing a safe, natural, economic, and

†To whom correspondence should be addressed.
E-mail: mohdyunus@upm.edu.my

comprehensive clean-up to remove several environmental contaminants [22,23]. Biosorption is defined as a physicochemical process for removing a substance (organic or inorganic) from a solution using a biological material or its components (dead or living) [24, 25]. Biosorption mechanisms include adsorption, absorption, surface complexation, precipitation, and ion exchange [17,26]. Biosorption has been seen to have a simple design, high performance, ease of operation, and low cost. Biosorption materials are widely available (e.g., agricultural and industrial wastes), and the process is swift and takes place between a few minutes to hours [27]. Many biosorption studies have been conducted with biomass of animals, plants and other by-products on metals, dyes, and substances alike [17,23]. However, as compared to bacterial biomass, many of these materials have a lesser surface area. As a result, the focus of this study is on employing bacterial biomass to address these problems.

The initial adsorbate concentration, agitation speed, the adsorbent surface area, temperature, contact time and the solution's initial pH all play a role in the liquid-solid interface process of adsorption [2,3,17]. To obtain the highest adsorption capacity and, as a result, the adsorbent's removal effectiveness, the process factors must be optimized [3,28,29]. The traditional method to process variable optimization is through a one-factor-at-a-time (OFAT) approach which necessitates a large number of trials, many of which are time-consuming, costly and laborious and usually neglect the possible interactions between multiple parameters, thereby putting the results at risk of being misinterpreted [30]. However, these drawbacks can be avoided by employing a statistical experimental design technique, which minimizes the number of trials while simultaneously providing an appropriate model for optimization that enables the assessment of the impact of inter-variable interactions on the process output [31,32]. Several forms of experimental design approaches have recently been used to optimize multivariable chemical processes [33]. RSM is a helpful approach for investigating the influence of multiple factors on responses by changing them all at once and doing a small number of trials [34]. In the literature, only a few studies used the optimization and experimental design modelling technique for the adsorption process [30,33]. Trypan blue is a dye used in the local textile industry that is often associated with dye pollution in the country [35,36]. Its removal using various methods by local researchers [37-39] indicates the urgency needed to remediate this pollutant. Bioremediation, chiefly biosorption, is one of the most economic and efficient methods of pollutant removal. Bacterial as biosorbent is an appealing agent for several reasons, including surface area, a variety of functional groups for sorption, uniformity in size and sustainable production using agricultural wastes [36]. Bacterial biomass, for example, AMT-Bioclaim™ was one of the earliest commercially available biosorbents for pollutants [38]. Bacterial biosorption of dye including Trypan Blue is thus a very attractive strategy in mitigating this pollutant. In this study we report on the sorption of Trypan Blue by *Pseudomonas* sp. strain MM02 inactivated biomass for the first time.

MATERIALS AND METHODS

1. Equipment, Chemicals and Reagents

The dye Trypan Blue used in this research was manufactured by Sigma Aldrich Co. USA. Other compounds used were of analytical grade quality and purchased from recognized dealers: Merck (Germany) and Fisher (Malaysia). A dye stock solution of 1,000 ppm for TB dye was made by diluting 1,000 mg of the dye salt in 100 mL of deionized water. All dye concentrations for the experimentation were reconstituted from the dye stock solution (1,000 ppm) using deionized water. The pH of the solution was modified with either 0.5 N HCl or 0.1 mol NaOH using a pH meter. The TB dye absorbance was standardized using a spectrophotometer (OD_{10} to OD_{1100} nm). The best absorbance peak was found between OD_{590} to OD_{640} nm [38].

2. Source of Bacteria

Twelve (12) different pure bacterial cultures (Isolate 34XR, Isolate 34XW, Isolate 52, Isolate 2, Isolate 1, Isolate 29, Isolate 7, Isolate 8, Isolate 4, Isolate 5.2, Isolate 30, and Isolate 5.1) were collected from Bioremediation, Biomonitoring & Ecotoxicology (BBE) Laboratory of the Faculty of Biotechnology and Biomolecular Sciences, Universiti Putra Malaysia. These bacterial isolates were initially isolated from Juru riversides in Pulau Pinang, Malaysia [10]. This area was reported to have a high concentration of pollutants originating from the textile industry [9]. Consequently, regular sub-culturing maintained a pure colony of each isolate under aseptic laboratory conditions in a nutrient broth (NB) and glycerol solution.

3. Harvesting Bacterial Biomass

The biomass of each of the twelve (12) isolates was harvested and screened for the potential adsorption of Trypan Blue dye. A day-old culture of the isolates of about 1 OD_{600} absorbance was centrifuged for 10 min at 10,000 rpm [39]. Each isolate's supernatant was discarded, and the pellets were washed twice with Tris Buffer at pH 7.0. To deactivate the cells, the pellets were inactivated at 60 °C in a steam bath after one hour [40]. The pellets were subsequently used for TB dye adsorption studies.

4. Screening of Bacterial Biomass

In a 50 mL flask, a volume of 10 mL of the dye TB was mixed with 0.22 g of each of the 12 inactivated bacterial biomass. The flasks were labelled accordingly and incubated at 25 °C temperature and 150 rpm. Two (2) mL aliquot of each flask was taken at a time interval (5 min), centrifugation was for 10 min at 10,000 rpm and examined using a spectrophotometer (OD_{620} nm) to monitor each bacterial biomass adsorption potential [41,42]. This step was repeated until the absorbance peak for each set of flasks became uniform. All experiments were performed in triplicates and the following formula (Eq. (1)) was used to compute the dye percentage adsorption;

$$\text{Dye percentage (\%) adsorption} = \frac{A - B}{A} \times 100 \quad (1)$$

where A represents initial absorbance before incubation, and B represents final absorbance after incubation.

The isolate with the highest adsorption percentage of TB dye was selected for further analysis.

5. Optimization of TB Dye Adsorption Using the One-factor-at-a-time (OFAT)

The above screening result revealed that Isolate 52 had the highest adsorption percentage of the TB dye. This isolate was already identified and characterized by Motharasan et al. [43], as *Pseudo-*

monas sp. strain MM02. As a result, the OFAT approach was used to improve the conditions for the adsorption of TB dye using the isolate *Pseudomonas* sp. strain MM02. Parameters optimized using the OFAT technique were the effect of dye concentration, pH, agitation speed, adsorbent amount, temperature and contact time. While keeping the optimized parameter(s) constant, each parameter was examined one after the other respectively. The experiments were all carried out in triplicate.

At several time intervals (0, 5, 10, 15, 20, 25, 30, 60, 120, 150, and 180 minutes), a batch experiment was set up to optimize the contact time effect on the adsorption of TB dye. An aliquot of the reaction mixture was obtained at each time interval and centrifuged for 10 minutes at 10,000 rpm in an Eppendorf. A spectrophotometer was used to evaluate the supernatant at a certain wavelength (OD620 nm) [16,44,45]. To determine the amount of dye adsorption impact as dye concentration increases, different dye concentrations were prepared for TB dye (5, 10, 15, 20, 30, 50, 70 and 90 ppm) [41]. The pH influences the chemistry of a solution. Therefore, the pH range examined for TB dye adsorption was between 5.0-8.0 (5.0, 5.5, 6.0, 6.5, 7.0, 7.5 and 8.0) [41,46]. An increase in agitation speed affects the adsorption rate of the dyes. Therefore, this parameter was checked on TB dye adsorption at 0, 50, 80, 100, 120, 150 and 170 rpm, respectively [26,47]. The biosorbent dosage heavily influences the extent of adsorption. The amount used was 0.11, 0.22, 0.43, 0.66, 0.88, 1.10, 1.76 and 2.20 g [45,48]. The effect of different temperatures was observed for the adsorption of TB dye ranging from 20, 25, 30, 35, 40 and 45 °C [49,50]. The supernatants were analyzed as described earlier and the results were processed accordingly.

6. Optimization of TB Dye Adsorption Using Response Surface Methodology (RSM)

Response surface methodology (RSM), unlike the OFAT, is being used to optimize and investigate interactions between multiple bioprocess parameters using a small number of experiments [31,32]. The RSM consists of several statistical and mathematical approaches for determining the relationship between response and independent variables [10,51]. So far, the RSM has been utilized to optimize numerous parameters in bioremediation processes with great success [32,52].

To use this optimization approach (RSM), two stages were involved, the Plackett-Burman Design (PBD) and the central composite design (CCD). The PBD optimization was to obtain the significant parameter(s) for the adsorption of dye TB. On the other hand, the significant parameter(s) obtained from the PBD optimization were further optimized using the CCD approach to enhance the adsorption capacity of the TB dye by the *Pseudomonas* sp. strain MM02 biomass [3,39]. The experimental design and statistical analyses for this RSM optimization (both PBD and CCD) were analyzed using Design-Expert 6.0.8 software [31].

6-1. Screening Using PBD

Six independent parameters affecting the adsorption of TB dye were screened according to the software, a total of 12 separate experimental runs were proposed. These experimental runs were predicted using the six different significant parameters from the OFAT optimization. Each parameter has a high value (+1) and low value (−1) and the adsorption percentage was given as the response in the PBD. Table 1 below presents the PBD experimental range and level design for TB dye adsorption. Analysis of variance (ANOVA) was carried out using the software and the parameters with $p<0.05$ were found significant and hence were further optimized using the CCD [10,53].

Table 1. Experimental range and level of independent variables tested using the PBD for TB dye

Factors	Variable	Unit	−1 (Low level)	+1 (High level)
A	Dye conc.	ppm	10	30
B	pH		6	7.5
C	Temperature	°C	25	40
D	Contact time	min	10	60
E	Adsorbent amount	g	0.22	1.1
F	Agitation rate	rpm	100	150

6-2. Optimization Using CCD

After the PBD optimization, the significant parameters were subsequently optimized via CCD. The significant parameters from the PBD were dye concentration, adsorbent amount and temperature. The maximum and minimum threshold for each of the significant parameters was dye concentration 3.18-30.82 ppm, temperature 19.89-45.11 °C, and adsorbent amount 0-1.25 g. The CCD was utilized to examine the PBD's significant parameters as well as the interaction between the variables [3,32]. A total of 20 sets of experimental runs were performed and all experiments were carried out in triplicate. Each experimental run's adsorptions percentage was computed and recorded as the dependent variable. The software's final projected RSM response was confirmed experimentally [51]. The correlation between the independent variables and the answer below was described using a second-order model (Eq. (2)) [3].

$$Y=\beta_0+\beta_1X_1+\beta_2X_2+\beta_3X_3+\beta_4X_4+\beta_{11}X_1+\beta_{22}X_2+\beta_{33}X_3+\beta_{44}X_4 +\beta_{12}X_1X_2+\beta_{13}X_1X_3+\beta_{14}X_1X_4+\beta_{23}X_2X_3+\beta_{24}X_2X_4+\beta_{34}X_3X_4 \quad (2)$$

where Y is a typical response parameter; and β_0, β_1, β_2, β_3, β_4, β_{11}, β_{22}, β_{33}, β_{44}, β_{12}, β_{13}, β_{23}, β_{24} and β_{14} are the model's constant regression coefficients, where β_0 is the intercept term, β_{11}, β_{22}, β_{33}, and β_{44} are the squared coefficients, β_{12}, β_{13}, β_{23}, β_{24}, and β_{14} are the interaction coefficients and β_1, β_2, β_3 and β_4 are the linear coefficients. X_1, X_2, X_3, and X_4 are the independent parameters. Parameter permutations (X_1, X_2) show the interaction among the variables.

6-3. Validation of Experiment

From the CCD results, the predicted adsorption response by the Design-Expert software was verified. The values of the most significant parameters given were used to validate the result of the experiment. Hence, the actual value of the percentage adsorption of the TB dye using *Pseudomonas* sp. strain MM02 biomass was obtained and compared with the predicted value given by the CCD [3].

7. Statistical Analysis

All experiments were carried out in triplicate, and the data was provided as mean standard deviation. To compare findings among groups, one-way ANOVA (95 percent confidence interval) in the SPSS statistics V. 25 software program (SPSS Inc., Chicago, Illinois, USA) was utilized, and Tukey's test was employed to conduct *post*

hoc pairwise comparison tests if significant differences were obtained. $P<0.05$ was determined to be statistically significant.

8. Kinetics, Isotherm, and Thermodynamic Models

This approach is like the one used in batch equilibrium investigations. The concentration of the solution of the absorbent-absorbate solution at various time intervals was determined. The quantity of adsorbed at time t, denoted by the symbol q_t (mg/g), was estimated using Eq. (3). q_t denotes the adsorption capacity by 1 gram of adsorbent at a certain time of exposure. The adsorption rate is assumed to be proportional to the difference between the adsorbed concentration and the number of accessible sites in the pseudo-first-order equation (PFO) proposed by Lagergren for solid-liquid systems [54]. A second-order relation between the adsorption rate and the difference between saturation concentrations is proposed in the pseudo-second-order model (PSO), which implies that chemisorption is the rate-limiting step [55].

The equation for Pseudo-first-order kinetic model

The pseudo-first-order kinetic model equation is as follows [60]:

$$q_t = q_e(1-e^{-k_1 t}) \tag{3}$$

The equation for the Pseudo–second-order kinetic model

The pseudo-second-order equation is as follows [55]:

The model is based on the adsorption capacity onto a solid phase [55] and the nonlinear form of PSO was initially proposed by Blanchard et al. [56]. It is expressed as:

$$q_t = \frac{k_t q_e^2 t}{1+k_2 q_e t} \tag{4}$$

The slope and intercept of the plot of t/q_t vs. t give the values of q_e and k_2, respectively.

Elovich kinetic model

The Elovich equation was originally developed to simulate the adsorption of carbon monoxide on the sorbent manganese dioxide. The Elovich model [57] is expressed as follows;

$$\frac{dq}{dt} = a\exp(-bq_t) \tag{5}$$

where b is surface coverage extent (g mg^{-1}) and chemisorption activation energy and a is the initial sorption rate (mg g min^{-1}).

For the biosorption isotherms, 17 isotherms models (Table 2) were utilized covering from one to five parameters models, and nonlinear regression instead of linear regression was carried out as the best model assessment using several error function analyses listed below. For the thermodynamic calculations, a dimensionless equilibrium constant was estimated from the Langmuir equation [58].

9. Thermodynamics Parameter Analysis

The Langmuir equation (Eq. (6)) was utilized to find the dimensionless equilibrium constant between two phases, K_L.

$$q_e = \frac{q_{mL} K_L C_e}{1+K_L C_e} \tag{6}$$

The K_L value from Langmuir was then converted to a dimensionless form K_C using Eq. (7) as follows [58]:

$$K_C = 980.6 \times 55.5 \times 1{,}000 \times K_L \tag{7}$$

The molecular weight of Evans blue is 980.6 $gmol^{-1}$. 55.5 is the molarity of pure water and the term of $980.6\times55.5\times1{,}000\times K_L$ will be dimensionless.

The dimensional constant K_L relation to the unitless equilib-

Table 2. Isotherm models utilized in this study

	Model	Formula
1	Henry's law	$q_e = HC_e$
2	Langmuir isotherm	$q_e = \frac{q_{mL} b_L C_e}{1+b_L C_e}$
3	Freundlich isotherm	$q_e = K_F C_e^{\frac{1}{n_F}}$
4	Temkin isotherm	$q_e = K_F C_e^{\frac{1}{n_F}}$
5	Jovanovic isotherm	$q_e = \frac{K_s q_{mS} C_e^{\frac{1}{n_S}}}{1+K_s C_e^{\frac{1}{n_S}}}$
6	Redlich-Peterson isotherm	$q_e = \frac{K_{RP} C_e}{1+\alpha_{RP} C_e^{\beta_{RP}}}$
7	Sips isotherm	$q_e = \frac{K_s q_{mS} C_e^{\frac{1}{n_S}}}{1+K_s C_e^{\frac{1}{n_S}}}$
8	Toth isotherm	$q_e = \frac{q_{mT} C_e}{\left(\frac{1}{K_T}+C_e^{n_T}\right)^{\frac{1}{n_T}}}$ $q = \frac{q_m p}{(b+p^t)^{1/t}}$ Where, $b = 1/K_t$.
9	Hill isotherm	$q_e = \frac{q_{mH} C_e^{n_H}}{K_H + C_e^{n_H}}$
10	Khan isotherm	$q_e = \frac{q_{mK} b_K C_e}{(1+b_K C_e)^{a_K}}$
11	BET isotherm	$q_e = \frac{q_{mBET}\alpha_{BET} C_e}{(1-\beta_{BET}C_e)(1-\beta_{BET}C_e+\alpha_{BET}C_e)}$
12	Vieth-Sladek isotherm	$q_e = K_{BS}C_e + \frac{q_{mVS} b_{VS} C_e}{(1+b_{VS}C_e)}$
13	Fritz-Schluender-III isotherm	$q_e = \frac{q_{mFS} K_{FS} C_e}{1+K_{FS} C_e^{n_{FS}}}$
14	UniLan isotherm	$q_e = \frac{q_{mU}}{2b_U}\ln\left(\frac{1+a_U C_e e^{b_U}}{1+Ca_{U_e} e^{-b_U}}\right)$
15	Baudu isotherm	$q_e = \frac{q_{mB} b_B C_e^{(1+x+y)}}{1+b_B C_e^{(1+x)}}$
16	Marczewski-Jaroniec isotherm	$q_e = q_{mMJ}\left(\frac{(K_{MJ}C_e)^{n_{MJ}}}{1+(K_{MJ}C_e)^{n_{MJ}}}\right)^{\frac{m_{MJ}}{n_{MJ}}}$
17	Fritz-Schluender-IV isotherm	$q_e = \frac{A_{FS} C_e^{a_{FS}}}{1+B_{FS} C_e^{b_{FS}}}$

rium constant of K_C is described in Eq. (8) where C^o is the selected standard of adsorbate (C^o=1 mol/L); K_L (L/mol) is the Langmuir constant and γ (dimensionless) is the activity coefficient of adsorbent in solution [64].

$$K_C \approx \frac{K_L\left(\frac{L}{mol}\right)\times C^o\left(\frac{mol}{L}\right)}{\gamma} \quad (8)$$

The van't Hoff equation was applied to determine the adsorption thermodynamics parameters (ΔG^o, ΔH^o and ΔS^o). The free energy change (ΔG) is nearly zero when the adsorption process reaches equilibrium. Then, Eq. (9) becomes the standard Eq. (10) which is routinely used to compute ΔG^o (standard Gibbs energy change) while Eq. (11) is the corresponding nonlinear form [59].

$$\Delta G^o = -RT\ln K_C \quad (9)$$

$$\ln K_C = \frac{-\Delta H^o}{R}\times\frac{1}{T}+\frac{\Delta S^o}{R} \quad (10)$$

$$K_C = e^{\frac{\Delta S^o}{R}-\frac{\Delta H^o}{R}\cdot\frac{1}{T}} \quad (11)$$

The universal gas constant, R is 0.00831 kJ/mol×K.

The connection among ΔG^o, ΔH^o and ΔS^o of an adsorption process is expressed as follows:

$$\Delta G^o = \Delta H^o + \Delta S^o \quad (12)$$

10. Statistical Analysis

For all models tested in this study, statistical discriminatory tests such as root-mean-square Error (RMSE), corrected AICc (Akaike Information Criterion), accuracy factor (AF) and bias factor (BF) and adjusted coefficient of determination (R^2) were utilized in this work. All the parameter estimations were made using CurveExpert 6.0.

The RMSE was calculated according to Eq. (13) where n is experimental data points, Ob_i and Pd_i are the experimental and predicted data, respectively, while p is parameter numbers.

$$RMSE = \sqrt{\frac{\sum_{i=1}^{n}(Pd_i - Ob_i)^2}{n-p}} \quad (13)$$

Since R^2 ignores models' parameter numbers, the adjusted R^2 is commonly used as it has a penalty for a number of parameters. In the equation (Eqs. (14) and (15)), the total variance of the y-variable is denoted by S_y^2 while RMS is the residual mean square.

$$\text{Adjusted}(R^2) = 1 - \frac{RMS}{s_Y^2} \quad (14)$$

$$\text{Adjusted}(R^2) = 1 - \frac{(1-R^2)(n-1)}{(n-p-1)} \quad (15)$$

The Akaike Information Criterion (AIC) AICc, which is based on the information theory [60] is calculated as follows (Eq. (16)).

$$AICc = 2p + n\ln\left(\frac{RSS}{n}\right) + 2(p+1) + \frac{2(p+1)(p+2)}{n-p-2} \quad (16)$$

Further error function analysis are the Accuracy Factor (AF) and Bias Factor (BF). (Eqs. (17) and (18)).

$$\text{Bias factor} = 10^{\left(\sum_{i=1}^{n} log\frac{(Pd_i/Ob_i)}{n}\right)} \quad (17)$$

$$\text{Accuracy factor} = 10^{\left(\sum_{i=1}^{n} log\frac{|(Pd_i/Ob_i)|}{n}\right)} \quad (18)$$

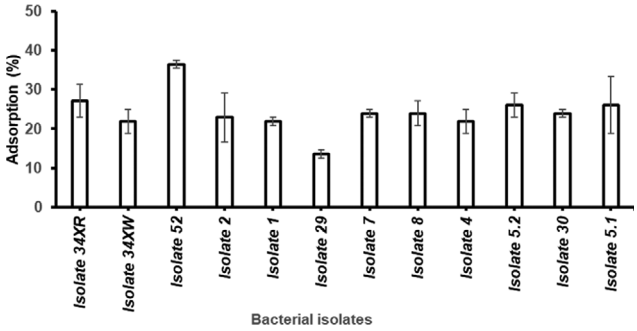

Fig. 1. Screening result showing the adsorption percentage of twelve (12) different bacterial isolates against TB dye.

RESULTS AND DISCUSSION

1. Bacterial Biomass Screening

Fig. 1 shows the screening result of the twelve (12) different bacterial isolates against the TB dye. All the 12 isolates show different adsorption percentages of the TB dye, Isolate 34XR 27%, Isolate 34XW 22%, Isolate 52 37%, Isolate 2 23%, Isolate 1 22%, Isolate 29 14%, Isolate 7 24%, Isolate 8 24%, Isolate 4 22%, Isolate 5.2 26%, Isolate 30 24%, and Isolate 5.1 26%. It was found that Isolate 52 had the best adsorption percentage of up to 37% among the other eleven (11) isolates. However, all the isolates showed the potential to adsorb the TB dye from the solution. Manogaran et al. [10] reported that most of these isolates show the ability to either decolorize or proliferate under Reactive Red 120 dye. Moreso, several studies previously reported the potential of bacterial biomass in the adsorption of different dyes [17,42,48,53].

Pseudomonas putida was employed by Ratnamala et al. [61] to investigate the biosorption of the dye Remazol Navy Blue. The researchers observed that *Pseudomonas putida* had a biosorption capacity of 20 mg of dye per gram of adsorbent, which was a significant finding. Isolate 52 was previously discovered and described as *Pseudomonas* sp. strain MM02 by [10]. Gram-negative, positive for citrate and nitrate reduction, negative for indole synthesis, urease, methyl red, VP, catalase, and oxidase. The partial sequence of the 16S ribosomal RNA gene from *Pseudomonas* sp. strain MM02 was 1,440 bp linear DNA with Accession number MW024071.1 GI: 1907461380 [43]. Bacteria are known to be global organisms that may be exploited in the environment as plentiful and affordable biosorbents. According to Karthik et al. [25], dyes were removed from water using bacteria such as *Pseudomonas*, *Bacillus*, *Streptomyces*, *E. coli*, and *Micrococcus*.

2. Optimization of TB Dye Adsorption Using the One-factor-at-a-time (OFAT)

The OFAT technique was used to investigate the effect of various environmental factors on the adsorption of TB dye, Fig. 2.

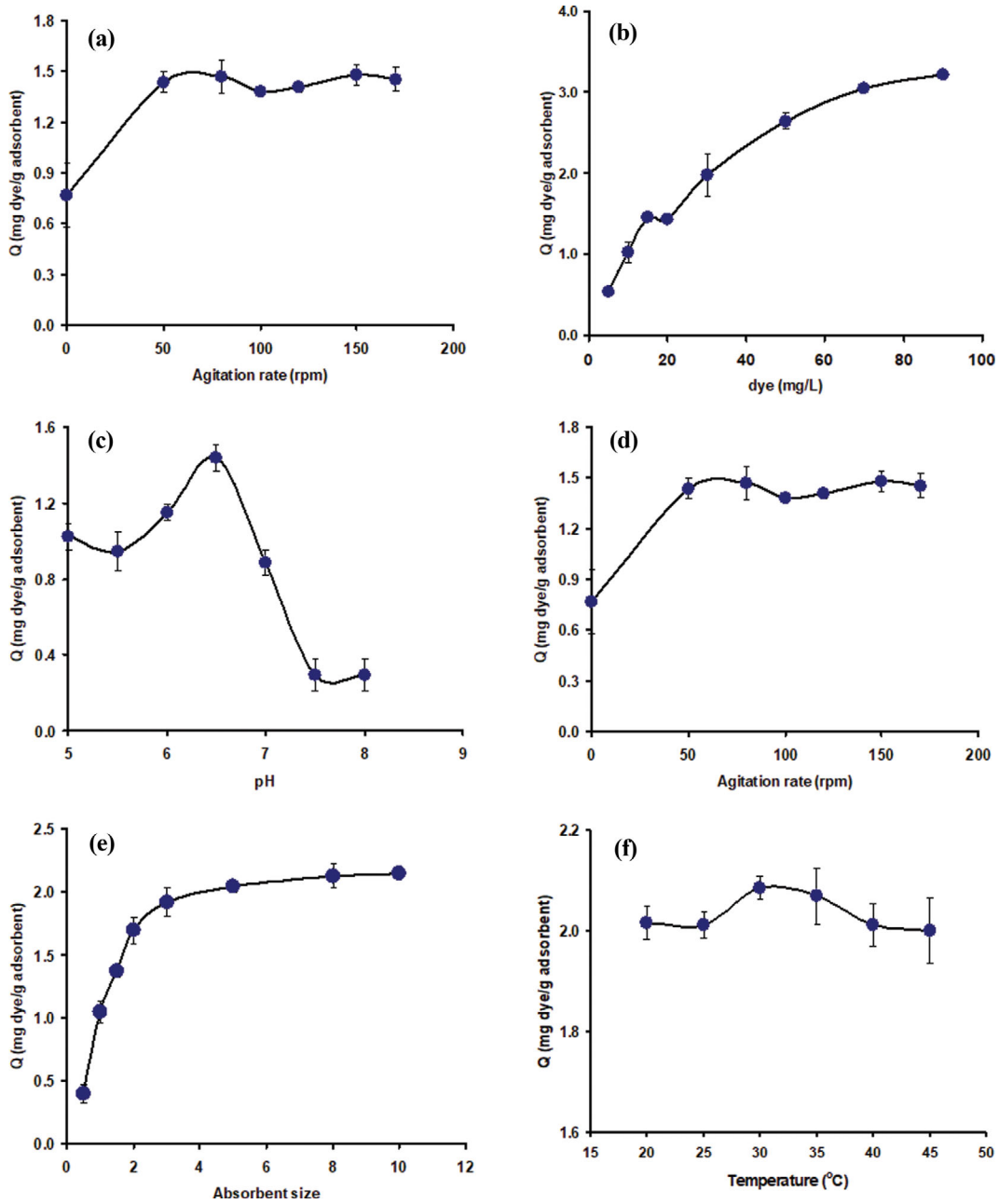

Fig. 2. OFAT optimization on the adsorption of TB dye by *Pseudomonas* sp. strain MM02; (a) Effect of contact time, (b) Effect of initial dye concentration, (c) Effect of pH, (d) Effect of agitation rate, (e) Effect of adsorbent amount, and (f) Effect of temperature.

2-1. Effect of Contact Time

In general, adsorption capacity rises with increasing time until it attains an equilibrium in which no more dye can be adsorbed from the solution. The amount of TB dye adsorbed is the highest dye adsorption capacity of the bacterial biomass under these settings. The equilibrium time is the time necessary to attain this state of equilibrium [62]. To investigate the contact time effect on the adsorption of TB dye, percentage dye adsorption was calculated at different time intervals between 0 and 180 min. Fig. 2(a) reveals that between 0 to 15 min, the percentage adsorption of the TB dye was below optimum. However, from 20 up to 180 min, the adsorption was at the optimum range. That is, the biosorbent has reached its adsorption time contact threshold. Furthermore, Fig. 2(a) shows that in the first 20 min the TB dye adsorption was fast, then followed by a slower phase until equilibrium was attained at around 25 min. Sufficient binding sites might explain this on the adsorbent (bacterial biomass) at the first phase. Over the contact period, dye removal was achieved from 32-37%. Several pieces of literature have reported that dye removal increases with contact time [16,44,45].

In a batch adsorption experiment, Rtanamala et al. [61] investigated the contact time effect modification on the percentage removal of Remazol Navy Blue. The initial biosorption was quick, but the adsorption progressed at a slower pace throughout the remainder of the experiment's duration. Because the initial bulk solution con-

centration was comparatively high, the driving forces were larger, resulting in higher rates as a consequence of the higher starting bulk solution concentration. After a period of time, the bulk concentration approached equilibrium and the rate of decay decreased. In another different example, Velkona et al. [46] looked at the influence of contact time on Methylene Blue and Congo Red biosorption by processing waste biomass of *Streptomyces fradiae* in a laboratory setting. The contact time range under investigation was between 5 and 180 min. According to their findings, the dye uptake was fast in the first 40 minutes, followed by a slow intermediate phase until equilibrium was established at 80 minutes for MB and 70 minutes for CR respectively. According to the researchers, the quick phase was caused by an excess of free binding sites on the biosorbent surface, while the second phase was caused by a restricted number of binding sites and a decline in the effectiveness of the system. All of these results were found to be consistent with the findings of the present investigation.

2-2. Effect of Initial Dye Concentration

As the dye amount adsorbed rises with increasing solution concentration at a given adsorbent dosage, the percentage of adsorption drops. That is, the number of adsorption sites decreases at increasing concentration, and dye removal becomes more dependent on the dye concentration (initial concentration) [62]. The potential of *Pseudomonas* sp. strain MM02 to endure higher dye concentration was investigated by conducting a batch experiment at different TB dye concentration from 5 to 90 mg/L shown in Fig. 2(b). The optimum adsorption of 36.28% was obtained at a concentration of 15 ppm of Trypan blue dye. One-way ANOVA revealed a significant actual difference between all the TB dye initial concentration classes (F (7, 16)=77.83, p<0.001).

Post hoc testing, however, indicated that there was no significant difference between the mean values for the optimum, 15 ppm and 10, 20 and 30 ppm (p>0.05). There were significant differences between 15 ppm and the remaining TB dye concentration tested (all p<0.001). The percentage adsorption decreases with a rise in the dosage of the TB dye (Fig. 2(b)). Still, the bacterial biomass was able to adsorb the TB dye even at 90 mg/L. This was owing to the mass transfer's strong driving force. The adsorption ability of the biosorbent increased as the initial TB dye concentration increased. Consequently, because of the surface saturation of the binding site on the biosorbent at increasing TB dye, the adsorption potential was reduced as seen in 50, 70 and 90 ppm, Fig. 2(b) [16, 46,63].

Several publications were in accord with the aforementioned conclusions about the influence of initial dye concentrations, which are detailed further below in this section. Jadhav et al. [64] reported that the bacteria *Pseudomonas aeruginosa* BCH decolorizes dye Acid Violet up to 98 percent in 30 minutes, with the amount of decolorization depending on the original dye concentration, temperature and pH used. A dye concentration of 250 mg/L was seen to be tolerable for the bacteria. In contrast, when the dye concentration was increased, the duration of time necessary for decolorization increased. Eventually, they came to the conclusion that the higher dye concentration might have compromised the enzyme system responsible for AV decolorization, leading to the extension of time required for decolorization. It was discovered in a similar study by El-Idreesy et al. [16] that the initial dye dosage had an effect on the final dye concentration. Initial dye concentrations of 2×10^{-5} M seem to be the most effective, removing 95.8 percent of the Trypan Blue in the process. Increased concentration of the dye would cause the equilibrium to change, favoring desorption rather than adsorption beyond this threshold, indicating that saturation has occurred at this point.

2-3. Effect of pH

Unlike other parameters, the pH influences the structural stability of dye molecules by altering the dye solution's chemistry and functional groups biosorbent's activity [49]. The pH influences the solution factors such as complexation by organic or inorganic ligands, hydrolysis, redox reaction and precipitation. The effects of pH on the bacterial biomass adsorption were investigated at various pH levels ranging from pH 5 to 8, and identified an optimum pH of 6.5. When the pH of the solution rises from 5.0 to 6.5, the TB dye removal increases from 26 to 38% (Fig. 2(c)). However, as the pH of the solution further increases to 8.0, the percentage of dye removal significantly decreases. Analysis of variance indicated a general significant difference between different pH values tested (F (7, 16)= 50.66, p<0.001). A *post hoc* test shows a significant discrepancy between the optimum pH 6.5 and all other pH tested (p<0.001). At low pH values, the surface of the biosorbent is often positively charged and it resists the biosorption of cationic species; however, when the solution's pH rises, the biosorbent surface becomes negatively charged, and electrostatic interactions between the oppositely charged sorbate and sorbent occur [46,49]. Velkova et al. [46] stated that the adsorption of basic dyes raises as the solution's pH rises. In contrast, the adsorption of acidic dyes decreases with an increase in the solution's pH. This proves Trypan Blue as an acid azo dye.

Several studies have demonstrated that the ideal pH for a large variety of biosorbents seems to be slightly acidic to neutral (pH 4-7), independent of whether the organisms are bacteria, fungi, algae, or yeast [41,65,66]. The solubility of ions may decrease with higher pH values in the solution, resulting in precipitation and complicating the sorption process [67]. On the basis of the common assumption that ions compete for the same spots on the biomass cell wall, fewer ions may be adsorbed when the pH is low. Ultimately, a broad spectrum of previous literature agreed on the importance of pH in dye biosorption, while also disagreeing on its significance.

2-4. Effect of Agitation Rate

In adsorption, agitation speed is a critical parameter. It affects the solute distribution in the bulk of the solution as well as the formation of an external surface layer. Generally, the degree of agitation affects the rate of dye adsorption and the adsorption increases as the stirring rate increases [62]. In addition, the agitation rate decreases resistance to the boundary layers and improves the system's mobility. Effects of agitation rate on the adsorption of TB dye by *Pseudomonas* sp. strain MM02 biomass was checked from the range of 0 to 170 rpm, Fig. 2(d). The TB dye adsorption was reviewed at 0, 50, 80, 100, 120, 150 and 170 rpm, respectively [26,47]. A review by Crini and Badot [62] reported two different kinds of literature where agitation rate had a high effect on dye adsorption and the order had little impact. This current research (Fig. 2(d)) shows that the effect of agitation rate has minor or no impact on

the TB dye adsorption, since it statistically shows no significant difference. The adsorption percentage was between 38 to 39%.

As previously reported by Pillai et al. [29], the isolate *Streptomyces* DJP15 degraded Azo Blue dye more effectively in a static condition (77.8 percent) than it did in an agitated environment (57.8 and 65.26 percent). In contrast, Shroff and Vaidya [68] evaluated the influence of sorbent/sorbate agitation speed (60-210 rpm) on Ni (II) adsorption. The removal effectiveness increased until the agitation speed reached 150 rpm (15.83 mg/g), after which the sorption capacity decreased as the agitation speed increased. For the simple reason that agitation encourages optimal interaction between biomass binding sites and metal ions. This decreases the thickness of the external mass transfer barrier around the adsorbent particles, allowing sorbate ion transport to the sorbent sites to be more efficient. As a consequence of the results, moderate agitation (150 rpm) was shown to optimize solid-liquid contact, resulting in the most homogeneous suspension possible. The decrease in efficiency associated with higher rotational speeds is due to ineffective interaction between ions and binding sites as a result of the creation of vortices in the suspension, which inhibits Ni (II) adsorption on the binding sites. Different research has revealed outcomes that are equivalent for a wide range of other contaminants.

2-5. Effect of Adsorbent Amount

The amount of biosorbent used has a significant impact on adsorption. Fig. 2(e) depicts the TB dye adsorption removal effectiveness by *Pseudomonas* sp. strain MM02 biomass. The adsorption efficiency of the biomass increased from 39% to almost 60% as the biosorbent amount was increased. The adsorbent amounts were 0.11, 0.22, 0.43, 0.66, 0.88, 1.10, 1.76 and 2.20 g [45,48]. The ANOVA result revealed a generally significant difference between different adsorbent amounts tested (F (7, 16)=349.16, p<0.001). After a *post hoc* comparison a significant difference was revealed between almost all the adsorbent amounts tested (p<0.001). According to Mane et al. [69], the wider the surface area, the more availability of the adsorption sites. On the other hand, the adsorption capacity declined due to biosorbent particle overlapping or aggregation.

The results of relevant research conducted by Hamzeh et al. [47] on dye removal, Remazol Black and Acid Orange using a new biosorbent revealed that increasing the biosorbent mass increased the percentage of dye removal from 41% to 51% for AO7 and from 41% to 95% for RB5, accordingly. There was an increase in the surface area of the adsorbent and, as a result, a rise in the number of active functional groupings, still resulting in more adsorbent surface availability. This may be linked to an increase in the percentage of removal. Because unsaturated adsorption sites are present throughout the adsorption process, increasing the amount of biosorbent used has a negative impact on the absorbance capacity of the sample. Increasing the amount of biosorbent used had no effect on the absorbance capacity of the sample. A further possibility is that particle aggregation, which occurs as a result of increased adsorbent mass, is responsible for the loss of absorbance capacity. Such aggregation would diminish the total surface area of the adsorbent while simultaneously extending the length of the diffusional pathway.

2-6. Effect of Temperature

The effect of different temperatures was observed for the adsorption of TB dye ranging from 20 to 45 °C, Fig. 2(f) [49,50]. The supernatants were analyzed as described earlier. The TB dye removal efficiency was optimum between the temperature range of 30 to 35 °C. Several works of literature documented that the amount of dye adsorption increases as the temperature rises because of the quick rate of diffusion provided by higher temperatures. In contrast, this finding (Fig. 2(f)) shows that between temperatures 20 to 25 °C and 40 to 45 °C, the adsorption percentage declined compared to a temperature between 30 to 35 °C. This might be explained by the fact that when the temperature rises, the solute's solubility increases and the contact forces between the solute and the solvent become greater than those between the solute and the adsorbent, making the solute more difficult to adsorb [70].

In the biosorption of Basic Red 46 by nickel oxide nanoparticles, increasing the temperature from 25 to 55 °C raises the adsorption percentage from 0.384 to 407 mmol/g [71]. In another investigation, the bacteria *Streptomyces* DJP15 sorption of Azo blue dye increased with increasing temperature, from 57 to 79 percent [29]. The temperature effect on the sorption of Malachite green by dry *Bacillus cereus* M116 cells was studied at 20, 30, 40, and 50 °C. The temperature changes were determined to have no influence on the biosorption process [72]. However, the temperature has a large impact on the adsorption process and the difference in sorption efficiency with regard to temperature change may be connected to the kind of sorption, such as chemical versus physical, as well as the modification of the functional group. As the temperature increases, the adsorbent's equilibrium capacity for a given adsorbate varies. Furthermore, a rise in temperature may speed the diffusion of dye molecules in the adsorbent's inner pores. Nonetheless, it was shown that some adsorption processes are not temperature sensitive [71].

Table 3 summarizes all the optimum conditions obtained from the optimization of TB dye adsorption using one-factor-at-a-time. The parameters optimized were contact time, dye concentration, agitation speed, solution pH, adsorbent amount, and temperature. The ideal setting for TB dye adsorption was found as follows: contact time 20 min, dye concentration 15 ppm, pH 6.5, an adsorbent amount 1.1 g, agitation speed 150 rpm and temperature 30 °C. Various optimization condition ranges for dye adsorption parameters have been described in the literature [10,51]. A one-factor-at-a-time strategy was employed by Lim et al. [51], to explore the influence of several factors on dye removal, and they discovered that the efficacy with which an azo dye decolorizes is strongly reliant on the kind of nutrients used and the quantity of inoculum used. It was discovered by Nath and Ray [72] that dried *Bacillus*

Table 3. Optimum conditions for the adsorption of Trypan Blue dyes

Parameters	Trypan blue
Contact time (min)	20.00
Dye concentration (ppm)	15.00
pH	6.50
Agitation speed (rpm)	150.00
Adsorbent amount (g)	1.10
Temperature (°C)	30.00

cereus M116 cells were effective in removing Malachite Green when used as a biosorbent. In the study, they discovered that the ambient circumstances had a major impact on the process. pH 5.0, 0.5 g/L biomass concentration, an initial dye concentration of 400 mg/L, and a duration of 360 minutes were found to be the most favorable conditions. Furthermore, a maximum absorption capacity of 485 mg/g of the dye was discovered. Similar to what many other studies have shown, this present study discovered that optimizing environmental conditions may considerably improve the adsorption process.

3. Optimization of TB Dye Adsorption Using Response Surface Methodology

The best conditions for TB dye adsorption were further optimized by using statistical approaches (Plackett-Burman, PBD and the central composite design, CCD techniques).

3-1. Optimization Using Plackett-Burman Design (PBD)

To screen and select key variables that influence the TB dye adsorption, the Plackett-Burman design was used. When two-way interactions are believed to be insignificant, this method is employed to examine the main effects. In a single experiment, the process may be used for many independent variables. However, only variables having significant impact on the TB dye adsorption were selected, for example, pH, dye concentration, temperature, contact time, adsorbent size and agitation speed. The ranges used for each of the independent components were based on the OFAT ranges, and a total of 12 tests employing stated factors were done in the PBD (Table 4). Salihu et al. [73], showed that first-order models were good fits for the PBD, which signifies second-order effects when the design involves center points. Based on the design matrix for screening significant variables, the lowest TB dye adsorption was found in run 9 (22.00%), while the highest adsorption was observed in run 5 (75.80%). The CCD was then used to optimize further the significant parameters found from the PBD.

Table 5 displays the first-order model's analysis of variance, as well as the model's regression analysis. The model was found highly significant and linear, with a slight curvature. pH and contact time were the only (marginally) insignificant parameter. Therefore, initial dye concentration, temperature, adsorbent amount and agitation speed are used in designing CCD. The model *F* value for TB was discovered to be 47.3, implying that the model was significantly based on ANOVA analysis (Table 5). There was only a 0.01% chance that a model *F*-value could occur because of noise. The model terms were discovered to be significant with a *p*-value <0.05. The coefficient of determination (R^2) was 0.9752, as shown by the

Table 4. Experimental design and percentage dye adsorption of TB dye in 12 experimental runs of Plackett-Burman design (PBD)

Run	A: Dye conc. (ppm)	B: pH	C: Temperature (°C)	D: Contact time (min)	E: Adsorbent size (g)	F: Agitation speed (rpm)	Adsorption (%)
1	30.00	6.00	25.00	10.00	1.10	150.00	68.87
2	10.00	7.50	25.00	10.00	0.22	150.00	45.10
3	30.00	7.50	25.00	60.00	0.22	100.00	24.79
4	30.00	7.50	25.00	60.00	1.10	100.00	61.43
5	10.00	6.00	25.00	60.00	1.10	150.00	75.82
6	30.00	7.50	40.00	10.00	1.10	150.00	53.17
7	10.00	6.00	40.00	60.00	1.10	100.00	66.01
8	30.00	6.00	40.00	10.00	0.22	100.00	23.69
9	30.00	6.00	40.00	60.00	0.22	150.00	22.04
10	10.00	7.50	40.00	10.00	1.10	100.00	74.51
11	10.00	7.50	40.00	60.00	0.22	150.00	41.83
12	10.00	6.00	25.00	10.00	0.22	100.00	43.14

Table 5. Analysis of Variance (ANOVA) for Trypan Blue dye adsorption from PBD

Source	Sum of squares	DF	Mean square	*F*-value	Prob>F	
Model	4,161.75	5	832.35	47.13	<0.0001	Significant
A	711.65	1	711.65	40.29	0.0007	
B	0.13	1	0.13	0.008	0.9336	
C	119.68	1	119.69	6.778	0.0405	
D	22.83	1	22.82	1.29	0.2990	
E	3,307.46	1	3,307.46	187.27	<0.0001	
Residual	105.97	6	17.66			
Cor total	4,267.72	11				
Std. Dev.	4.20	R^2	0.9752			
Mean	50.03	Adj R^2	0.9545			
C.V.	8.40	Pred R^2	0.9007			
PRESS	423.88	Adeq precision	18.48			

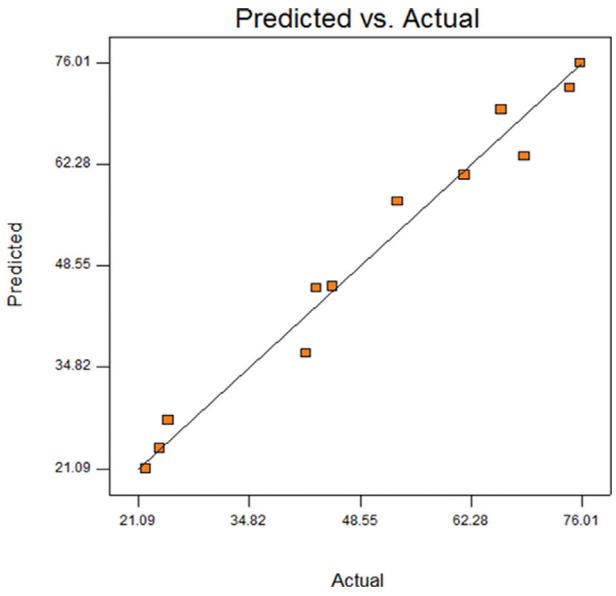

Fig. 3. Similarity plot between actual and predicted adsorption values for TB dye adsorption using *Pseudomonas* sp. strain MM02 in PBD.

ANOVA, firmly fitted in the regression line. The adjusted and the predicted R^2 values were discovered to be 0.9545 and 0.9007. Hence, the adjusted and the predicted R^2 values were in reasonable agreement. The adequate precision value that measures signal to noise was 18.48, presenting a suitable and sound signal. Fig. 3 presents the similarity plot between the predicted and the actual PBD value recorded, which can be expressed as Eqs. (19) and (20), respectively:

$$Y=55.20-0.77A+0.14B-0.42C-0.05D+8.30E \quad (19)$$

$$Y=50.03-7.70A+0.11B-3.16C-1.38D+16.60E \quad (20)$$

Plackett-Burman design was used by Manogaran et al. [10] to screen for critical factors influencing Reactive Red 120 decolorization by the bacterial consortia JR3, with decolorization levels ranging from 36.7 to 85.7 percent in 12 experimental tests. The ANOVA indicated that the dye concentration (A), the temperature (C), and the Reactive Red120 concentration (D) were all significant ($p<0.05$); however, the pH (B) was not significant ($p>0.05$). Statistically significant results were yielded from the model for pH correlations with dye concentration (AB), temperature (BC), and Reactive Red120 concentration (BD) ($p<0.05$). A favorable interaction in this stipulation was made possible by the inclusion of all four components, which were regarded as key model requirements. As shown by a low probability value obtained from the *F*-test (*F* value=428.70), the quadratic regression model was highly significant according to the results of the ANOVA of the model. Also shown by the study was a high level of agreement between the "Predicted *R*-squared" value of 0.9972 and that of 0.9329 after the model was adjusted, demonstrating the model's effect on the results. A fundamental composite design was created as a consequence of incorporating all four of these characteristics.

3-2. TB Dye Adsorption Optimization Using Central Composite Design (CCD)

The CCD model was used to produce the best response within the parameters' defined range. Also, the model enables the complicated response function to be determined by a small number of variables. The optimum values for the variables were obtained by solving the regression equation and evaluating the response sur-

Table 6. Experimental plan and result for the optimization of Trypan Blue adsorption using central composite design, CCD

Run	A: Dye concentration (ppm)	B: Temperature (°C)	C: Adsorbent size (g)	Experimental value (%)	Predicted value (%)
1	20.00	32.50	0.66	61.34	50.09
2	10.00	25.00	1.10	62.09	64.10
3	20.00	32.50	0.66	45.00	50.09
4	10.00	40.00	1.10	73.54	76.08
5	20.00	32.50	0.66	48.26	50.09
6	10.00	40.00	0.22	32.68	35.66
7	20.00	32.50	0.00	0.00	1.02
8	30.00	40.00	1.10	57.00	57.82
9	30.00	25.00	1.10	54.17	51.49
10	20.00	32.50	0.66	49.31	50.09
11	20.00	45.11	0.66	57.64	55.03
12	20.00	32.50	1.25	65.51	64.06
13	3.18	32.50	0.00	66.67	62.64
14	30.00	40.00	0.22	15.83	14.13
15	36.82	32.50	0.66	30.33	33.92
16	10.00	25.00	0.22	33.33	32.82
17	20.00	32.50	0.66	50.69	50.09
18	20.00	32.50	0.66	45.83	50.09
19	20.00	19.89	0.66	45.14	47.32
20	30.00	25.00	0.22	19.17	16.93

face contour plots. The CCD model was used to further optimize the significant parameters found in the PBD model. Twenty (20) different experimental designs with six center points were carried out as shown in Table 6.

The individual and interaction impacts of the specified process factors on the TB dye adsorption by the produced magnetic nanocomposite solution were investigated using a CCD method. The highest adsorption capacity for TB dye was found to be in run 4 (76.08%). The accuracy of a model is estimated by the determination coefficient (R^2). Borugadda and Goud [74] reported that the R^2 value is between 0 and 1, and its order of magnitude indicates the model's goodness between the predicted and model experimental response variable values. The R^2 value of the model was found to be 0.9624, which was closer to 1, which shows that there is only 96.24% model behavior that can be interpreted for the adsorption while the model cannot explain only 3.76% of the full variance. It also revealed that the regression model explained the majority of the data variance.

Furthermore, the model's relevance was demonstrated by a relatively high value of the adjusted and predicted R^2 values of 0.9285 and 0.8725 (Table 7), respectively, which demonstrates a strong correlation between actual and anticipated values. Consequently, the models illuminated the relationship between the response variable and the independent variables. Other researchers have found a similar trend in second-order RSM studies using Box Behnken and central composite designs [3,75,76]. The signal-to-noise ratio tested by adequate precision was found to be 21.06, thus indicating a good signal. This value highlights the model's significance for the process. It was necessary to have a ratio of greater than four. Manogaran et al. [75] reported an adequate precision score of 31.14 for the statistical optimization of culture component for the mineralization of glyphosate by the bacterium *Burkholderia vietnamiesis* strain AQ5-12.

The significance of model parameters is often measured using the *F*-value or *P-value* ("Prob>*F* value). Hassanzadeh-Tabrizi and Taheri-Nassaj [77] reported that the higher the size of the *F*-value and the correspondingly lesser the "prob>*F* value, the most essential is the corresponding coefficient. The model was shown to be very significant using the quadratic regression model, with *F*-value of 28.40 and a probability value that is extremely low 0.0001. Similarly, there was barely a 0.01% possibility that a model *F*-value this big could occur due to noise. The 'Prob>*F*' <0.0500 values specify that the model terms were significant. In this case, A, C and C^2 model terms were significant for the adsorption of Trypan Blue dye by *Pseudomonas* sp. strain MM02 inactivated biomass. The lack of fit, *F*-values and *P*-values of the model were 0.45 and 0.80, respectively. The lack of fit was not significant, indicating that the model was correct without any noise. Manogaran et al. [75] and Ibrahim et al. [78] found no significant lack of fit and regarded the model as an excellent fit.

The results obtained were consistent with the findings of Ibrahim et al. [78], who also utilized the response surface methodology (CCD) to further optimize critical parameters revealed in PBD. According to their findings, a total of 30 separate tests were carried out, and it was discovered that the model's R^2 value was 0.9422, which was close to one, and that 94.22 percent of the model's behavior could be explained, with only approximately 5.78 percent of the total variance remaining unaccounted for. In general, an R^2 value that is exceptionally close to 1 indicates that the data is well-matched. It was discovered that the model provided a reasonable explanation of the interactions between the independent variables and response variables, which proved to be a significant advantage. RSM has been demonstrated to enhance the results of a variety of optimization studies; however, artificial neural networks (ANNs), machine learning, and the Taguchi method are just a few of the different optimization techniques that may be found in the

Table 7. CCD-RSM analysis of variance (ANOVA), Trypan Blue

Source	Sum of squares	DF	Mean square	*F*-value	Prob>F	
Model	6,496.98	9.00	721.89	28.40	<0.0001	Significant
A	995.44	1.00	995.44	39.17	<0.0001	
B	71.82	1.00	71.82	2.83	0.12	
C	4,797.48	1.00	4,797.48	188.76	<0.0001	
A^2	5.87	1.00	5.87	0.23	0.64	
B^2	2.13	1.00	2.13	0.08	0.78	
C^2	554.46	1.00	554.46	21.82	0.00	
AB	15.95	1.00	15.95	0.63	0.45	
AC	5.36	1.00	5.36	0.21	0.66	
BC	41.72	1.00	41.72	1.64	0.23	
Residual	254.16	10.00	25.42			
Lack of fit	79.26	5.00	15.85	0.45	0.80	Not significant
Pure error	174.90	5.00	34.98			
Cor total	6,751.14	19.00				
Std. Dev.	5.041	R^2	0.9624			
Mean	45.68	Adj R^2	0.9285			
C.V.	11.04	Pred R^2	0.8725			
PRESS	860.67	Adeq precision	21.06			

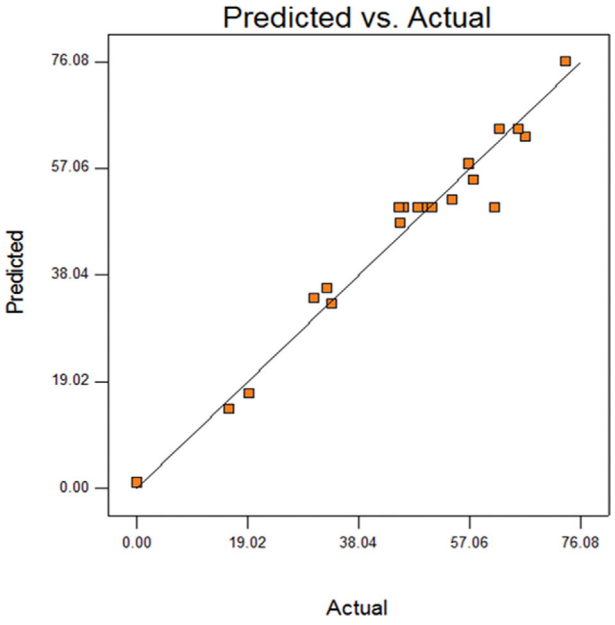

Fig. 4. Experimental and predicted factors for optimal responses for TB dye adsorption.

literature.

Fig. 4 depicts the similarity between the actual and predicted values for TB dye adsorption acquired in the CCD. The actual and anticipated model values had a significant relationship. Eqs. (21) and (22) describe these in terms of actual and coded factors, respectively:

$$Y=24.89-0.11A-0.22B+12.91C-0.007A^2+0.007B^2-1.55C^2 -0.019AB+0.04AC+0.15BC \quad (21)$$

$$Y=50.09-8.54A+2.29B+18.74C-0.64A^2+0.38B^2-6.20C^2 -1.41AB+0.82AC+2.28BC \quad (22)$$

4. 3D Response Surface Plot for Trypan Blue Dye Adsorption

The three-dimensional (3D) response surface plot of the dependent variable as a function of two independent factors reveals information about their relationships. Additionally, it aids in the understanding of both the main and interaction impacts of the two independent variables [3]. To further understand the influence of the independent factors and their interaction on the dependent variable, 3D response surface plots for the dignified answers were constructed using the quadratic model. The three unique process parameters' effects on the response parameter are depicted in 3D response surface graphs.

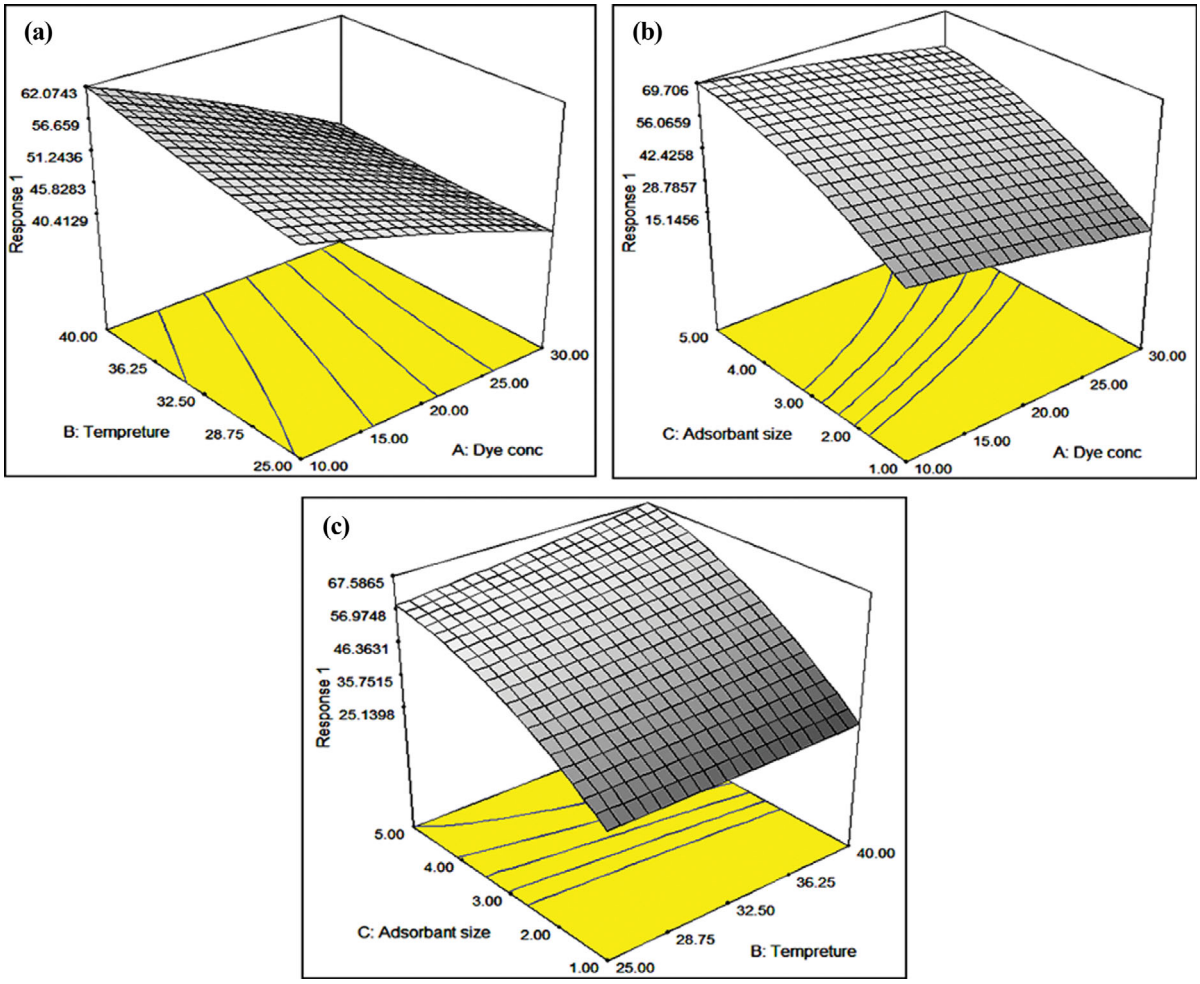

Fig. 5. Three-dimensional response surface plots for the TB dye adsorption showing the interactive effects between (a) temperature and initial TB dye concentration, (b) adsorbent size and dye concentrations, (c) adsorbent size and temperature.

Fig. 5(a) reveals the cumulative impact of TB dye concentration and temperature on the dye adsorption at a constant adsorbent size (0.66 g). The TB dye adsorption increases with both the temperature and dye concentration within their appropriate experimental arrays. Singh et al. [3] reported that a rise in temperature might increase the number of dye molecule binding sites on the adsorbent surface, explaining the temperature dependency of the adsorption. The interaction effect between the adsorbent size and the initial concentration of the dye at a given temperature of 32.50 °C showed an important effect (Fig. 5(b)). It indicates that TB dye adsorption increases as the adsorbent size increases and decreases in dye concentration within the experimental ranges. The observed drift may be described by an increase in the dosage, which makes more adsorption sites accessible. When paired with a constant dye concentration, it results in a decreased adsorption rate due to a smaller concentration differential between the solution bulk and the adsorbent contact. The concentration gradient will be comparatively high for the low adsorbent dosage, resulting in a greater adsorption rate. Fig. 5(c) presents the adsorbent size and temperature interactive effect at a constant TB dye concentration of 20.00 ppm. In the experimental range, adsorption increases with increasing concentration at lower temperature, whereas at higher temperature, adsorption decreases with increasing concentration. This is explained by the fact that raising the adsorbate concentration while keeping the dye concentration constant causes saturation of the surface binding sites at lower temperature, resulting in a decline in adsorbate uptake with increasing concentration, whereas at higher temperature as the number of binding sites grows, the sorption process improves.

5. Validation of RSM Experiment

The CCD-RSM result was used to validate the quadratic model. The best conditions for TB dye adsorption were found to be 22.27 ppm TB dye concentration, 34.27 °C temperature and adsorbent size of 0.32 g, whereas the other parameters were held constant in accordance with OFAT, since they were not significant from the PBD analysis. RSM predicted a 50.09% adsorption. An experiment was then done using the ideal parameters described above to validate the CCD estimation. Table 8 shows a comparison of the anticipated output by RSM and that obtained experimentally, revealing no statistically significant change in percentage adsorption between the experimental and predicted values (t-test, $p>0.05$). Jadhav et al. [79] discovered that the observed and predicted values were quite comparable, indicating that RSM was a success. Similarly, in this validation, RSM has also been shown to be a successful method for improving the TB dye adsorption by bacterial biomass, as shown by the results of the study.

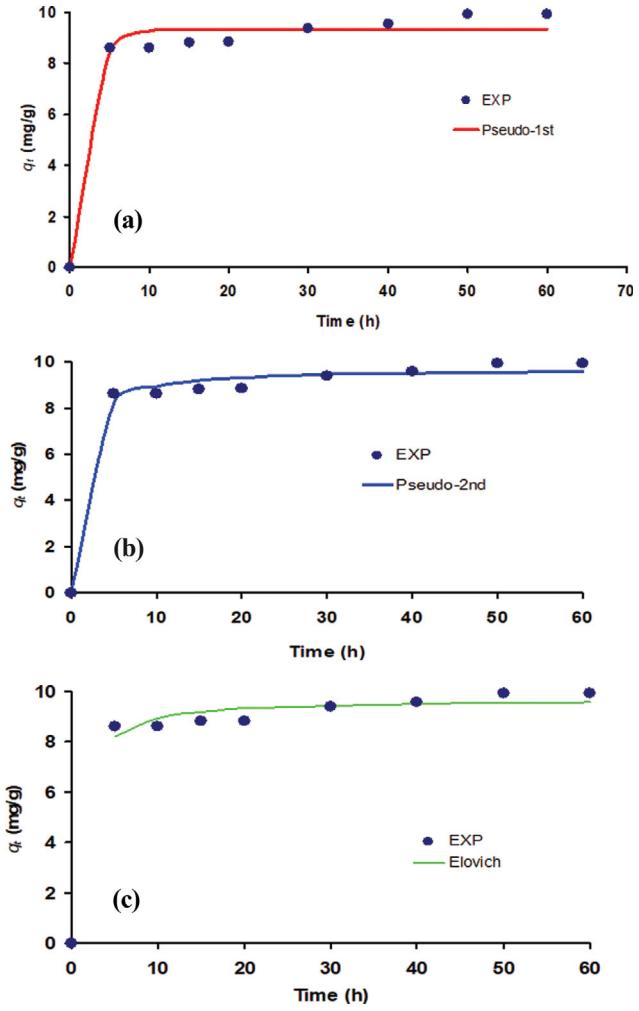

Fig. 6. Kinetics of 100 mg/L TB dye adsorption using *Pseudomonas* sp. strain MM02 as modelled using the pseudo-first order (a), pseudo-second order (b) and Elovich (c) models (data at time zero is omitted due to natural logarithm transformation restriction).

6. Kinetics, Isotherms, and Thermodynamic Models

6-1. Determination of Kinetic Model for Batch Adsorption Studies

Kinetic analysis involved using three models: pseudo-first order (PFO), pseudo-second (PSO) and Elovich (Fig. 6). Since the linearization of nonlinear data disturbs the data's error structure, this makes it harder to assess uncertainty, which is often reported as 95% confidence interval range [80]. Hence, non-linear regression is preferable for kinetic model fitting, since it is conducted on the

Table 8. Comparison between the predicted generated adsorption from RSM and experimental result

Factors	Name	Predicted levels	Experimental levels
A	Dye Conc. (ppm)	22.27	22.27
B	Temperature (°C)	34.27	34.27
C	Adsorbent size (g)	0.32	0.32
		Predicted	Experimental
Response (%)		50.08521	61.51

Table 9. Statistical analysis for TB dye adsorption using *Pseudomonas* sp. strain MM02 adsorbent at 100 mg/L dye

Model	RMSE	R^2	adR^2	AICc	BIC	HQC	AF	BF
Pseudo-1st order	0.494	0.978	0.970	−0.17	−10.58	−11.82	1.040	1.001
Pseudo-2nd order	0.349	0.989	0.985	−6.40	−16.80	−18.05	1.029	1.000
Elovich	9.865	−0.129	−0.505	53.74	43.34	42.09	1.016	1.000

Table 10. Model constants for the kinetics study of TB dye adsorption using *Pseudomonas* sp. strain MM02 adsorbent at 100 mg/L dye

Pseudo-1st order			Pseudo-2nd order			Elovich		
	Value	(95% C.I.)		Value	(95% C.I.)		Value	(95% C.I.)
q_e	9.329	8.875 to 9.783	q_e	9.725	9.245 to 10.204	b	1.632	0.994 to 2.271
k_1	0.48	0.185 to 0.774	k_2	0.113	0.021 to 0.206	a	94,915	−426,973 to 616,804

same abscissa with a linear regression plot, showing more accurate calculations.

Considering the statistical indicators, pseudo-second order is more accurate in describing the biosorption kinetic profiles than PFO and Elovich based on error functions analysis with the lowest RMSE and AICc, adjusted R^2 nearest to 1.0 and bias and accuracy factors near unity (Table 9). Kinetic analysis using the PSO model at 100 mg/L of TB dye gives a value of equilibrium adsorption capacity, q_e of 9.725 mg g^{-1} (95% confidence interval (C.I.), 9.245 to 10.204) (Table 10). It was inferred that the three kinetics models discovered to be suitable for fitting the current adsorption kinetics data are as follows: Pseudo-second order>Pseudo-first order> Elovich. As far as TB dye biosorption is concerned, the PSO model is also the best model for several adsorbents such as mesoporous orange peel [81], modified Luffa sponge with zinc nanoparticles [82] and avocado seed powder, while pseudo-first order was the best model for the crosslinked soy polysaccharide-based hydrogel nanostructure [83].

The pseudo-second order model was utilized to fit data for all TB concentrations, and the data showed excellent agreement with the pseudo-second order equation (Fig. 7).

It is often accepted that the ability to fit the kinetic data is the best test of the PFO and PSO equations' validity, despite the fact that such a test has little to do with whether or not the equations have a solid physicochemical foundation. Both k_1 and k_2 are phenomenological rate constants that decline when the adsorbate concentration is raised at the outset. k_1 and k_2 values variy widely from measurement to measurement, making it difficult to draw conclusions about the underlying physics and chemistry and extrapolate valuable results. The PFO and PSO equations may be fitted to most kinetic data even if the experimental conditions affecting the adsorption kinetics are not completely controlled. The PFO equation typically gave lower estimates of q_e than did the experiments. This mismatch was due to a delay in the onset of the adsorption process, which was likely brought on by the existence of a boundary layer or external resistance regulating. In the adsorption process that followed the PSO equation, the chemical reaction was not always the rate-limiting step because a good fit alone is not enough to reveal the true nature of the rate-limiting step [84,85].

6-2. Adsorption Isotherm Model

All 17 isotherms models were fitted to the data (Fig. 8). Based on Table 11, the Sips isotherm model was found to be the best fit model out of the 17 fitted isotherm models used in the current investigation with an adjusted R^2 value of 0.99, lowest values for RMSE

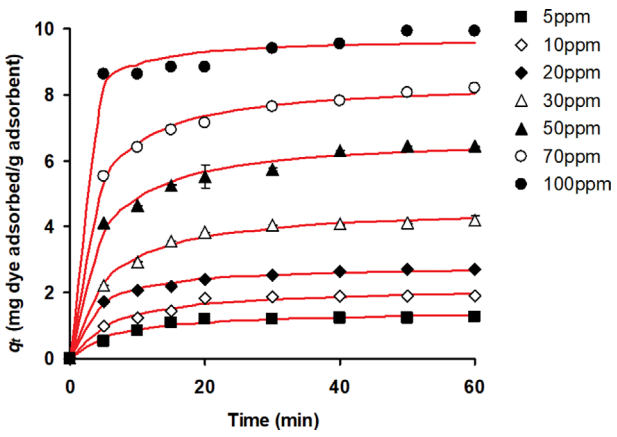

Fig. 7. Experimental data versus calculated data (line) on pseudo-second-order kinetic analysis of TB dye adsorption using *Pseudomonas* sp. strain MM02 as modelled using the pseudo-second order.

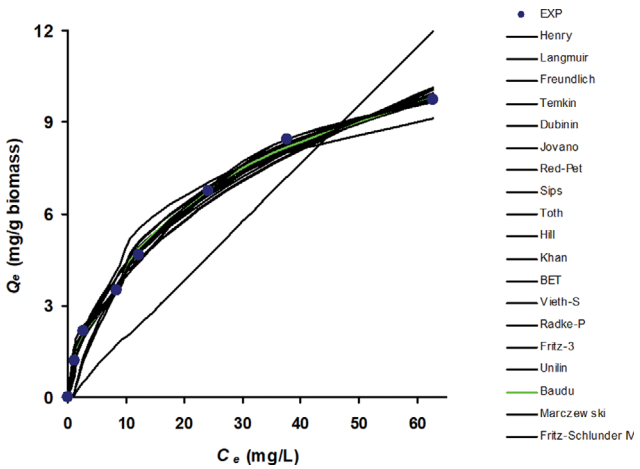

Fig. 8. A summary plot of experimental data and all the selected isotherms models fitted for the TB dye adsorption using *Pseudomonas* sp. strain MM02.

Table 11. Error functions analysis of 17 selected isotherm models for the TB dye adsorption using *Pseudomonas* sp. strain MM02

Model	p	RMSE	adR2	AICc	BIC	HQC	BF	AF
1. Freundlich	2	0.335	0.988	−3.78	−3.78	−15.62	1.05	1.07
2. Hill	3	0.195	0.996	−2.57	−2.57	−23.66	1.02	1.04
3. Redlich-Peterson	2	0.401	0.984	−0.90	−0.90	−12.75	0.95	1.10
4. Khan	3	0.237	0.994	0.57	0.57	−20.53	1.02	1.04
5. Vieth-Sladek	3	0.237	0.994	0.57	0.57	−20.53	1.02	1.04
6. UniLan	3	0.246	0.994	1.11	1.11	−19.99	0.99	1.04
7. Langmuir	2	0.556	0.973	4.31	4.31	−7.53	0.74	1.37
8. BET	3	0.302	0.991	4.40	4.40	−16.70	0.98	1.05
9. Toth	3	0.305	0.990	4.57	4.57	−16.52	0.99	1.06
10. Temkin	2	0.594	0.963	5.36	5.36	−6.48	0.96	1.14
11. Jovanovic	2	0.601	0.969	5.55	5.55	−6.29	0.71	1.41
12. Fritz-3	3	0.367	0.985	7.56	7.56	−13.54	1.05	1.07
13. Sips	3	0.433	0.981	10.20	10.20	−10.90	0.94	1.11
14. Marczewski	4	0.167	0.997	13.84	13.84	−25.84	1.03	1.04
15. Fritz-Schluender IV	4	0.170	0.997	14.06	14.06	−25.62	1.02	1.04
16. Baudu	4	0.195	0.996	16.28	16.28	−23.40	1.02	1.04
17. Henry	1	1.836	0.778	17.06	17.06	10.73	0.47	2.26

and AICc, while values of accuracy factor (AF) and bias factor (BF) closest to unity. The Sips isotherm is generated by combining both the Langmuir and Freundlich isotherm models in a single equation.

Table 11 is the list of isotherms models, of which the Freundlich and the Hill models share a similar performance based on error function analysis, such as smallest RMSE, adjusted correlation coefficient, accuracy factor and bias factor nearest to unity for Hill and smallest AICc, HQC and AICc values for the Freundlich model. The Freundlich model is empirical and cannot predict the maximum adsorption n which K_F ($(mg\ g^{-1}{\cdot}L\ mg^{-1})^{1/n}$) is the Freundlich isotherm constant, and n_F is the Freundlich exponent. As the $1/n_F$ value was small and approaches zero, the system is heterogenous [84-86] and is predictable for bacterial surfaces. As the Freundlich equation is unable to model the maximum adsorption, the Halsey rearrangement of the Freundlich equation gave the estimated maximum absorption of 10.118 mg g^{-1}, which is very close to the experimental value. Similar works using bacteria as adsorbents are rare in the literature for TB sorption. The bacterium *Aeromonas hydrophila* RC1 shows maximum adsorption (Langmuir) for TB of 0.75 mg g^{-1} [48], *Trichoderma harzianum* shows maximum adsorption (Langmuir) of 2.33 mg g^{-1} [87], while in another study using corn zein, a maximum adsorption of 4 mg g^{-1} TB was achieved [87], of which *Pseudomonas* sp. strain MM02 performed better than these biosorbents. The maximum adsorption predicted by the Langmuir model was 12.097 mg g^{-1} (95% confidence interval from 10.197 to 13.996), which is lower but comparable with other nonbacterial sorbents for TB such as avocado seed powder [15] and crosslinked soy polysaccharide-based hydrogel nanostructure [83] with maximum adsorptions of 19.3 (Langmuir) and 37.52 mg g^{-1} (Langmuir), respectively (Table 12). Much higher maximum adsorption capacity of 45.32 and 47.3 mg g^{-1} was reported for Luffa sponge (LS) and modified Luffa sponge with zinc nanoparticles (ZnNPs) for LS and LS-ZnNPs, respectively [82]. Table 13 below, present a summary of Trypan Blue (TB) and dyes sorption systems by bacteria and other biosorbents.

6-2-1. Theory

Isotherm studies

Dye molecules in the aqueous phase reach a dynamic equilibrium with those on the adsorbent surface under isothermal conditions during the adsorption process, and this equilibrium is expressed by the isotherms. These adsorption isotherms allow for a straightforward estimation of the optimal loading of adsorbents [88]. The most fitted isotherms, which are system dependent, provide a better explanation of the adsorbent-adsorbate binding. Adsorption equilibrium has been modelled in various ways. The following are explanations of the best isotherm models in this study, including the Langmuir and Freundlich models, two models often reported in adsorption studies.

Henry isotherm

When solutes are adsorbed onto a uniform adsorbent surface at low enough concentrations that all solute molecules are separated from their nearest neighbors, Henry's equation provides a good fit. The amount of adsorbate at the surface is shown to be directly proportional to the concentration of the adsorbate, making this the simplest type of adsorption isotherm. This isotherm provides a linear relationship between the equilibrium concentrations in the fluid phase and the adsorbed phase:

$$q_e = HC_e \tag{23}$$

where H (L mg^{-1}) is the adsorption equilibrium constant known as the Henry constant. As H rises, the adsorbent and solute molecules interact more strongly.

Langmuir isotherm

In the Langmuir isotherm, adsorbate is adsorbed to the homogeneous adsorbent surface in a monolayer manner. The isotherm presumes that all adsorption sites are the same and have the same energy, and the adsorbent is structurally homogeneous for monolayer adsorption to occur [89]. This isotherm model predicts the

Table 12. Isothermal models' constants for the TB dye adsorption using *Pseudomonas* sp. strain MM02

	Model	Parameters	Unit	Value	(95% confidence interval)
1	Henry's law	H	L mg^{-1}	0.192	0.134 to 0.250
2	Langmuir isotherm	q_{mL}	mg g^{-1}	12.097	10.197 to 13.996
		b_L	L mg^{-1}	0.059	0.035 to 0.083
3	Freundlich isotherm[#]	K_F	(mg g^{-1}·L mg^{-1})$^{1/n}$	1.476	1.187 to 1.764
		n_F	(L mg^{-1})	2.149	1.896 to 2.402
		q_{mF}*	mg g^{-1}	10.118	
4	Temkin isotherm[‡#]	K_T	L mg^{-1}	1.150	0.877 to 1.423
		b_T	J mol^{-1}	1.021	0.360 to 1.682
5	Jovanovic isotherm	q_{mJ}	mg g^{-1}	9.612	8.153 to 11.070
		K_J		0.059	0.036 to 0.082
6	Redlich-Peterson isotherms	K_{RP}	L mg^{-1}	1.827	−0.024 to 3.677
		β_{RP}	dimensionless	0.670	−0.481 to 1.820
		α_{RP}	L g^{-1}	0.666	0.505 to 0.828
7	Sips isotherm	q_{mS}	mg g^{-1}	0.059	0.032 to 0.085
		K_S		20.997	8.533 to 33.461
		n_S		1.525	1.142 to 1.908
8	Toth isotherm	q_{mT}	mg g^{-1}	43.527	−42.768 to 129.822
		K_T		0.476	0.044 to 0.907
		n_T		0.310	0.000 to 0.620
9	Hill isotherm	q_{mH}	mg g^{-1}	20.997	8.534 to 33.460
		n_H		0.656	0.491 to 0.820
		K_H		17.025	9.284 to 24.766
10	Khan isotherm	q_{mK}	mg g^{-1}	2.527	−0.321 to 5.375
		b_K		0.555	−0.446 to 1.556
		a_K		0.609	0.484 to 0.734
11	BET isotherm	q_{mBET}	mg g^{-1}	8.263	5.301 to 11.225
		α_{BET}		0.110	0.031 to 0.189
		β_{BET}		0.004	0.000 to 0.008
12	Vieth-Sladek isotherm	q_{mVS}	mg g^{-1}	6.841	3.633 to 10.049
		b_{VS}		0.138	0.020 to 0.256
		K_{VS}		0.060	0.015 to 0.106
13	Fritz-Schluender-III isotherm	q_{mSF}	mg g^{-1}	2.728	0.743 to 4.714
		K_{FS}	L mg^{-1}	0.670	−0.481 to 1.820
		nF_S		0.666	0.505 to 0.828
14	UniLan (Unilin) isotherm*	q_{mU}	mg g^{-1}	1.108	−716.480 to 718.696
		a_U		5.820	−3.445 to 3.447
		b_U		0.001	−3,760.33 to 3,771.97
15	Baudu isotherm	q_{mB}	mg g^{-1}	171.753	−2,238.425 to 2,581.930
		b_B		0.007	−0.090 to 0.103
		x		−0.012	−2.427 to 2.403
		y		−0.396	−3.121 to 2.330
16	Marczewski-Jaroniec isotherm	q_{mMJ}	mg g^{-1}	9.792	9.053 to 10.532
		K_{MJ}		0.020	0.018 to 0.022
		n_{MJ}		9.067	−20.812 to 38.945
		m_{MJ}		0.516	0.485 to 0.546
17	Fritz-Schluender-IV isotherm	A_{FS}		1.248	1.037 to 1.459
		a_{FS}		0.541	0.453 to 0.628
		B_{FS}		0.000	−0.000 to 0.001
		b_{FS}		2.106	−1.315 to 5.526

*Isotherms with ln term should not be plotted using data that starts from the origin (0,0)

[‡]Isotherms having an RT term should be plotted using the temperature (Kelvin) studied

[#]Isotherms that have no direct way in estimating maximum adsorption capacity (mg g^{-1})

Table 13. Summary of Trypan Blue (TB) and dye sorption systems by bacteria and other biosorbents

Adsorbent (bacterial biomass)	Sorbate (dye)	Best kinetics	Best isotherm	Adsorbent dose g/L	Dye removal (mg/g)	Reference
Aeromonas hydrophila RC1	Trypan Blue	20-80	Langmuir	1.5	0.75 mg/g	[48]
Avocado seed powder	Trypan Blue	0-76.8	Langmuir	0.016	19.3 mg/g	[16]
Crosslinked soy polysaccharide-based hydrogel nanostructure	Trypan Blue	Pseudo-2nd order (linearized)	Langmuir		37.52 mg/g	[83]
Luffa sponge (LS)	Trypan Blue	Pseudo-2nd order (Linear)	Langmuir	1	47.3 mg/g	[82]
Live and autoclaved Mycelium of *Trichodema harzianum*	Trypan Blue		Langmuir	1 g/50 mL	2.32 and 2.33 mg/g	[87]
Pennisetum purpureum	Coomassie Brilliant Blue G250	Pseudo-2nd-order		1 g/L	40 mg/g	[20]
Rhodopseudomonas palustris 51ATTA strain	Fast Black K		Langmuir	1 g/L	142.86 mg/g	[140]
Rhodopseudomonas sp. strain 51ATA	Astrazon Red		Freundlich and Langmuir	1 g/L	5.51 mg/g	[49]
Nostoc linckia HA 46	Reactive Red 198	Pseudo-2nd-order		100 mg/L	93.5 mg/g	[141]
Corynebacterium glutamicum	Reactive Black 5 (RB%)	Pseudo-2nd-order	Redlich-Peterson and Sips	500-2,000 mg/L	419 mg/g	[17]
Rhodococcus erythropolis AW3	Crystal violet (CV)	Pseudo-2nd-order	Langmuir	0.5 g/L	289.8 mg/g	[39]
Aeromonas hydrophila RC1	Eriochrome Black T	Pseudo-1st-order	Freundlich	1.5 g/L	451.8 mg/g	[48]
Aeromonas hydrophila RC1	Acid Red	Pseudo-1st-order	Langmuir	1.5 g/L	58.8 mg/g	[48]
Pseudomonas sp. strain DY1	Acid black 172	Pseudo-2nd-order		0.05 g	333.46 mg/g	[125]
Bacillus megaterium	Reactive blue 5	First and the second order	Langmuir	0.05 g	163.93 mg/g	[41]
Bacillus subtilis HAU-KK01	Congo red	Pseudo-2nd-order	Freundlich	1%		[50]
Paenibacillus macerans	Acid Blue 225 (AB 225) and Acid Blue 062 (AB 062)	Pseudo-2nd-order	Langmuir	1 g/L	95.08 mg/g	[142]
Bacillus thuringiensis (Bt) 016	Methylene blue			25 mg/L		[134]
Streptomyces fradiae	Congo Red (CR) and Methylene Blue (MB	Pseudo-2nd-order	Freundlich and Langmuir	2 g dm^{-3}	59.63 mg/g	[46]

existence of monolayer coverage of the dye at the outer surface of the adsorbent due to the exponential decay of intermolecular forces with increasing distance. This model predicts a constant monolayer adsorption capacity and simplifies the linear Henry's model for both low and high solute concentrations [90]. Expression of the Langmuir Isotherm is as follows:

$$q_e = \frac{q_{mL} b_L C_e}{1 + b_L C_e} \tag{24}$$

where q_{mL} (mg g^{-1}) is the maximum monolayer adsorption capacity, and b_L (L mg^{-1}) (together with q_{mL}) are the Langmuir model constants. Weber and Chakravorti suggested R_L, which is a separate factor, to determine the affinity between the sorbate and sorbent whether it is favorable or unfavorable [91]. The equation is as follows:

$$R_L = \frac{1}{1 + C_e b_L} \tag{25}$$

An alternative to the Brunauer-Emmett-Teller (BET) method for calculating the surface areas of porous solids is the Langmuir iso-

therm [92]. BET isotherm model can be reduced to Langmuir isotherm if the adsorbent surface is assumed to be homogeneous and completely coated by dye molecules. Therefore, the specific surface area S_{sp} ($m^2\ g^{-1}$) of the adsorbent may be determined using the following equation, which requires knowledge of the maximal monolayer adsorption capacity (q_{mL}) determined using the Langmuir equation and the predicted area of a dye molecule A (nm^2).

$$S_{sp} = \frac{6.023 \times 10^{23} \times A \times q_{mL}}{1{,}000} \tag{26}$$

Freundlich isotherm

When it comes to adsorption, the empirical Freundlich isotherm model is more accurate in describing reality than the idealized Langmuir isotherm, which is limited to the formation of a monolayer. This relationship helps to explain the phenomenon of multilayer adsorption, in which affinities and adsorption heat are not distributed uniformly over the heterogeneous adsorbent surface [93]. The equation is as follows [93]:

$$q_e = K_F C_e^{\frac{1}{n_F}} \tag{27}$$

in which K_F ($(mg\ g^{-1} \cdot L\ mg^{-1})^{1/n}$) is the Freundlich isotherm constant, and n_F is the Freundlich exponent. Where C_e is the adsorbent's equilibrium concentration ($mg\ L^{-1}$), q_e is the amount adsorbed per unit mass of the adsorbent ($mg\ g^{-1}$), K_F and n_F are Freundlich constants, of which the latter predicts how favorable the adsorption process is. The amount of toxicant adsorbed onto the adsorbent at a unit equilibrium concentration is denoted by the adsorption capacity, K_F ($mg\ g^{-1}\ (L\ mg^{-1})^{1/n}$), which may also be thought of as the distribution coefficient. Adsorption intensity, or surface heterogeneity, is quantified by the slope of $1/n_F$. The Langmuir isotherm is approached when $1/n_F$ is less than 1, and the presence of cooperative adsorption of a surface is indicated when $1/n_F$ is greater than 1. A more heterogeneous system will have a $1/n_F$ value approaching zero while a more homogeneous system will have a $1/n_F$ value approaching unity [85]. The big drawbacks of the Freundlich equation are its inability to model the maximum adsorption [94] and being an empirical rather than mechanistic model. To estimate the maximum adsorption capacity, the Halsey rearrangement of the Freundlich equation allows us to use the final data point of C_e as an estimate:

$$K_F = \frac{q_{mF}}{C_e^{\frac{1}{n_F}}} \tag{28}$$

Notice that the term q_e has now been changed to q_{mF}. The maximum adsorption capacity is an estimate only.

Jovanovic isotherm

This model's consideration of an adsorption surface assumption is comparable to Langmuir's. The second approximation for localized monolayer adsorption in the absence of lateral interactions corresponds to this scenario. The main distinction between this model and the Langmuir model is that the surface binding vibrations of an adsorbed species are considered [95]. The equation is as follows [93]:

$$q_e = q_{mJ}(1 - e^{-K_J C_e}) \tag{29}$$

where maximal adsorption capacity in the Jovanovic model, expressed in milligrams per gram (mg/g), is denoted by q_{mJ}. Assumptions similar to those of the Langmuir isotherm were used by Jovanovic [95] when this model was developed, which additionally considers the surface binding vibrations of the adsorbed species. One further approximation for lateral-interaction-free monolayer localized adsorption is the Jovanovic isotherm. At very high concentrations, it follows the Langmuir isotherm instead of Henry's law [93]. For Jovanovic's local behavior, this isotherm predicts a quasi-Gaussian function with a bias toward high adsorption energies. To get the equivalent Jovanovic equation for multilayer adsorption (three parameters) [95], the equation is as follows:

$$q_e = q_{mJ}(1 - e^{-K_{J1} C_e}) e^{K_{J2} C_e} \tag{30}$$

Redlich-Peterson isotherm

The features of both the Freundlich and Langmuir isotherms are incorporated into the three-parameter model. This model is a mixture of the two; therefore the adsorption mechanism does not follow the rules of ideal monolayer adsorption [96]. Numerous applications exist for the Redlich-Peterson isotherm model, which includes homogeneous and heterogeneous systems. The equation is as follows [93]:

$$q_e = \frac{K_{RP} C_e}{1 + \alpha_{RP} C_e^{\beta_{RP}}} \tag{31}$$

where K_{RP} is the Redlich-Peterson model isotherm constant ($L\ mg^{-1}$), a_{RP} is the Redlich-Peterson model constant ($L\ g^{-1}$), and b_{RP} is the Redlich-Peterson model exponent, which should be in the range 0 to 1. Redlich-Peterson equation is reduced to the Henry equation at b_{RP}=0 and to the Langmuir equation at b_{RP}=1. Adsorption equilibrium is represented by a linear dependence on concentration, which holds true over a wide concentration range. This is because the numerator is based on the Langmuir isotherm model, which allows it to enter the Henry zone at infinite dilution [97]. To solve the equations, this isotherm model uses a minimal approach. This method optimizes the degree to which the theoretical model's predictions agree with the points in the experimental data [98].

Toth isotherm

Using an empirically modified version of the Langmuir equation, this isotherm model attempts to minimize the discrepancy between the experimental and projected values. This isotherm model is commonly employed for the modelling of heterogeneous adsorption systems, as it adequately accounts for both low and high adsorbate concentrations. This isotherm model assumes a non-normal distribution of adsorption energies, where the majority of sites have energies that are lower than the mean or the peak [99]. The equation is as follows [100]:

$$q_e = \frac{q_{mT} C_e}{\left(\frac{1}{K_T} + C_e^{n_T}\right)^{\frac{1}{n_T}}} \tag{32}$$

where K_T and n_T are the Toth isotherm constant and exponent, respectively, and q_{mT} ($mg\ g^{-1}$) is the maximal monolayer adsorption capacity predicted by the Toth isotherm. K_t is related to the

binding energy. The n_T scale measures the degree of surface variation. It follows from the Langmuir isotherm equation that the process takes place on a homogeneous surface if n_T approaches unity. Therefore, (n_T) is a parameter that represents the heterogeneity of the adsorption system; the system is deemed heterogeneous when (n_T) is not equal to the unity value [101]. Furthermore, as a result of the independent association between temperature and the parameter n_T, an increase in temperature causes a quick increase in K_T.

The Toth isotherm model's equation is preferred over Sips' because it can characterize the data's behaviour at both high and low concentrations. Do [102] states that the slope of this isotherm model is constant at zero loading but begins to decrease at a given loading at a pace significantly faster than that for the Langmuir equation. The effect of heterogeneity, as measured by n_T, is responsible for this. As the adsorption process continues, molecules are physically attracted to higher-energy sites, but as the adsorption proceeds, they are attracted to lower-energy sites, resulting in a sluggish increase in the adsorbed amount vs concentration than that is predicted by the Langmuir equation.

Sips isotherm model

The Sips isotherm model was developed by fusing the Langmuir and Freundlich isotherm models in order to forecast the heterogeneity of the adsorption systems and to avoid the restrictions associated with the rising concentrations of the adsorbate in the Freundlich model. Next, an expression with a finite limit at a high concentration is generated. The Sips model is correct because it effectively localizes the adsorption without involving the adsorbate-adsorbate interaction [103]. The equation is as follows [93]:

$$q_e = \frac{K_s q_{mS} C_e^{\frac{1}{n_s}}}{1 + K_s C_e^{\frac{1}{n_s}}} \tag{33}$$

where K_S (l/g) and q_{mS} (mg/g) are the Sips isotherm constant and maximum monolayer adsorption capacity, respectively. n_S is the Sips model exponent. However, the Sips isotherm model deviates from Henry's law since it reduces to the Freundlich model at low adsorbate concentrations. However, the monolayer adsorption feature of the Langmuir model is predicted at high adsorbate concentrations. The equation's parameters are controlled by operational conditions such as changes in pH, concentration and temperature [104]. The primary flaw of the Sips model is the same as that of the Freundlich model: when pressure (or concentration) is low, neither model predicts the accurate Henry's law limit [102].

The Hill isotherm model

The Hill equation was suggested to explain the binding of various species onto and adsorbent's homogeneous substrates. The model is derived from the non-ideal competitive adsorption model. The model assumes that the adsorption process followed a cooperative event in which the binding ability of a ligand at one site on a macromolecule can affect the binding capacity of other sites on the same macromolecule [105]. The equation is as follows [93]:

$$q_e = \frac{q_{mH} C_e^{n_H}}{K_H + C_e^{n_H}} \tag{34}$$

Maximum uptake saturation (in mg/L) as determined by the Hill isotherm, q_{mH}, the Hill constant (K_H), and the Hill cooperativity coefficient (n_H) of the binding interaction (dimensionless). Binding is cooperative if $n_H>1$, non-cooperative or hyperbolic if $n_H=1$, and non-cooperative if $n_H<1$.

Temkin isotherm

Adsorption is defined by a uniform distribution of bonding energies up to a maximum binding energy in the Temkin isothermal model, which was developed by Temkin and Pyzner [106]. The indirect adsorbate-adsorbate interactions on heterogeneous surfaces cause the heat of adsorption of all molecules in the layer to drop linearly with the amount of surface covering. The Temkin isotherm is constructed with the Langmuir adsorption isotherm as its foundation. Adsorption is an exothermic process, as evidenced by the positive heat of adsorption ($b_T>0$). The popular Temkin model as follows is not correct due to the dimension issue between the left and the right parts of the equation.

$$q_e = \frac{RT}{b_T}\{\ln(a_T C_e)\} \tag{35}$$

This has been highlighted and the correct Temkin model is as follows [107];

$$\frac{q_e}{q_{mT}} = \frac{RT}{b_T}(\ln(K_T C_e)) \tag{36}$$

In this equation, K_T is the adsorption equilibrium constant of the solute on the solid surface expressed as L mg^{-1}, solute equilibrium concentration (C_e) is mg L^{-1}, q_e and q_m are the equilibrium and saturated adsorption amount and expressed as mg g^{-1}, while b_T has a unit of J mol^{-1} and represents the adsorption heat parameter.

Khan isotherm

The adsorption of solutes from diluted aqueous solutions has been modelled using a generalized equation by Khan et al. [108]. This isotherm is notable in that it encompasses both the Langmuir and the Freundlich isotherms. This model of the isotherm was created for both single and binary and ternary systems. The equation follows:

$$q_e = \frac{q_{mK} b_K C_e}{(1 + b_K C_e)^{a_K}} \tag{37}$$

Where

The maximum monolayer adsorption capacity q_{mK} is expressed in mg g^{-1}, b_K and a_K are Khan isotherm constant and Khan isotherm exponent, respectively. The preceding equation simplifies to the Langmuir isotherm for $a_K=1$, and to the Freundlich isotherm for large values of C_e [93].

BET isotherm

The BET equation [109] describes the equilibrium adsorption of a gas onto a solid surface and is a specific variant of the Langmuir Isotherm. This model depicts the adsorption phenomena onto a homogeneous surface following the successful development of a monolayer, and it accounts for multilayer adsorption without ignoring the requirements of Langmuir isotherm. It is essential to be aware of the fact that the traditional BET equation for gas phase adsorption, which makes the assumption of unlimited adsorption at saturation concentration, cannot be applied to the process of adsorption that takes place in the liquid phase. Since both the adsor-

bate and the solvent are already in condensed form, the amount of adsorption will not increase with increasing liquid phase concentration if the adsorbent does not have an affinity for the adsorbate or if it is already saturated with the adsorbate [110]. Non-microporous adsorbent surfaces can be described by this isotherm, making it a useful tool for physisorption. The BET isotherm equation is

$$q_e = \frac{q_{mBET}\alpha_{BET}C_e}{(1-\beta_{BET}C_e)(1-\beta_{BET}C_e+\alpha_{BET}C_e)} \quad (38)$$

where q_{mBET} (mg g^{-1}), α_{BET} and β_{BET} are the maximum monolayer adsorption capacity and the dimensionless BET isotherm constants, respectively.

Vieth-Sladek isotherm

While working on a new method of estimating diffusion rates in solid adsorbents from transient adsorption, Vieth-Sladek constructed a model with a unique two-part component: a linear segment (Henry's law) and a non-linear segment (the one most typically come across) (Langmuir isotherm). The linear part describes how molecules stick to locations on the porous surfaces of the adsorbent by a process called physisorption, whereas the non-linear part shows the adherence of molecules to porous surface sites of the adsorbent [111]. The equation [112] is as follows;

$$q_e = K_{VS}C_e + \frac{q_{mVS}b_{VS}C_e}{(1+b_{VS}C_e)} \quad (39)$$

where q_{mVS} (mg g^{-1}) is the maximum monolayer adsorption capacity, b_{VS} and K_{VS} are the Vieth-Sladek adsorption equilibrium and model constant, respectively.

Fritz-Schluender-III isotherm

Fritz and Schluender propose an empirical expression that, thanks to a high number of coefficients in their isotherm, can accommodate a wide variety of experimental data [113]. Fritz-Schluender isotherm-III [114] has the following form:

$$q_e = \frac{q_{mFS}K_{FS}C_e}{1+K_{FS}C_e^{n_{FS}}} \quad (40)$$

where the maximum monolayer adsorption capacity is q_{mFS} (mg g^{-1}). K_{FS} (L mg^{-1}) and n_{FS} are the Fritz-Schluender-III equilibrium constant and model exponent. respectively. Fritz-Schluender-III reduces to the Freundlich model for large adsorbate concentrations, but changes to the Langmuir model if n_{FS}=1.

UniLan (Unilin) isotherm

Unilan is another one empirical correlation mentioned in the book by Valenzuela and Myers which was suggested for the equilibrium data analysis. The name Unilin is also utilized in some publication where the term UniLan should be used instead. The term UniLan comes from "Uniform distribution and Langmuir local" isotherm. The Unilan equation assumes a patch-wise surface, with the local Langmuir equation valid on each patch [115]. This isotherm [116] is represented as:

$$q_e = \frac{q_{mU}}{2b_U}\ln\left(\frac{1+a_UC_e e^{b_U}}{1+Ca_{U_e}e^{-b_U}}\right) \quad (41)$$

where q_{mU} (mg g^{-1}) is the maximum monolayer adsorption capacity predicted by Unilan isotherm, a_U and b_U are the Unilan equilibrium constant and model exponent, respectively. b_U characterizes the heterogeneity of the system. The larger the value of this parameter, the system becomes more heterogeneous. If b_U=0, in this limit, the value for the range of energy distribution becomes zero, and the UniLan equation is converted to the classical Langmuir equation.

Baudu Isotherm

Measurements of tangents at various equilibrium concentrations allow for the determination of the Langmuir coefficients, b_L and q_{mL}, which demonstrate that these parameters are not constants throughout a wide concentration range. This prompts Baudu to develop a new model as follows:

$$q_e = \frac{q_{mB}b_BC_e^{(1+x+y)}}{1+b_BC_e^{(1+x)}} \quad (42)$$

This holds true only inside the intervals (1+x+y)<1 and (1+x)<1. Specifically, the maximal monolayer adsorption capacity predicted by the Baudu isotherm is denoted as q_{mB} (mg g^{-1}), b_B, x and y are the Baudu equilibrium constant and exponents of the Baudu model.

Marczewski-Jaroniec isotherm

This four-parameter generalized Langmuir equation isotherm follows the assumptions of Langmuir's isotherm [117]. This isotherm model simplifies to the Langmuir isotherm if n_{MJ} and m_{MJ} are equal to 1, and to the Langmuir-Freundlich isotherm if n_{MJ}= m_{MJ}. The assumption of the local Langmuir isotherm model and the distribution of adsorption energy in the active sites on the adsorbent is the principal premise of this isotherm model. This isotherm is given as:

$$q_e = q_{mMJ}\left(\frac{(K_{MJ}C_e)^{n_{MJ}}}{1+(K_{MJ}C_e)^{n_{MJ}}}\right)^{\frac{m_{MJ}}{n_{MJ}}} \quad (43)$$

where the maximum monolayer adsorption capacity predicted by Marczewski-Jaroniec isotherm is q_{mMJ} (mg g^{-1}). K_{MJ}, n_{MJ} and m_{MJ} are the Marczewski-Jaroniec equilibrium constant and model expo-

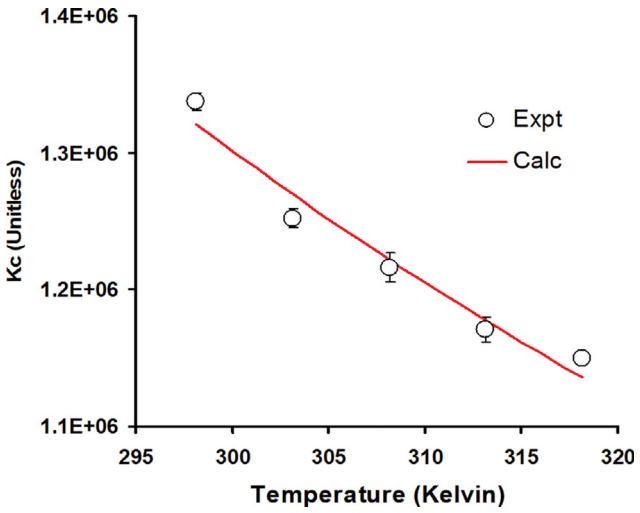

Fig. 9. Nonlinear plot of K_c (dimensionless form of Langmuir's K_L) vs temperature for the TB dye adsorption using *Pseudomonas* sp. strain MM02.

Table 14. Thermodynamic parameters for the adsorption of the TB dye on *Pseudomonas* sp. strain MM02

T (°C)	T (K)	K_c Coefficient distribution method			
		ΔG^o (kJ mol^{-1}) (95% C.I.)		ΔH^o (kJ mol^{-1}) (95% C.I.)	ΔS^o (J mol^{-1}) (95% C.I.)
25	298.15	−34.94	−34.99 to −34.89	−5.96 (−6.74 to −5.17)	97.20 (94.65 to 99.74)
30	303.15	−35.39	−35.45 to −35.33		
35	308.15	−35.91	−36.00 to −35.81		
40	313.15	−36.39	−36.48 to −36.30		
45	318.15	−36.92	−36.96 to −36.89		

nents, respectively.

Fritz-Schluender-IV isotherm

Increasing the number of parameters for an isothermal model usually allows a better fitting to a complicated curve. Fritz and Schluender developed empirically such a model [113]. It is expressed by the equation;

$$q_e = \frac{A_{FS} C_e^{a_{FS}}}{1 + B_{FS} C_e^{b_{FS}}} \quad (44)$$

where a_{FS} and b_{FS} are the Fritz-Schluender-IV model exponents, and A_{FS} and B_{FS} are the Fritz-Schluender-IV equilibrium constants. All possible values for these exponents are less or equal to one. The Fritz-Schluender-IV isotherm reduces to the Freundlich equation at high aqueous phase concentrations of solute. This isotherm reduces to the Langmuir isotherm when a_{FS}=b_{FS}.

6-3. Thermodynamic Studies

As the van't Hoff plot is modelled using a nonlinear form (Fig. 9), the negative values for the ΔG^o and ΔH^o (Table 14) indicate that the sorption process is spontaneous and exothermic, respectively.

The low magnitude of ΔH^o, which is less than 40 KJ/mol, indicates the sorption process is via a physisorption route rather than a chemisorption [118], of which for the latter, a magnitude of between 80-400 kJ/mol is expected [119]. The relatively low magnitude of ΔG^o also supports physisorption as the magnitude for chemisorption is often reported between −400 to −80 kJ/mol [56]. In addition, the capacity of adsorption tends to decrease with an increase in temperature [120], which was observed in this study. Physisorption is also the dominant process for several bacterial sorptions of dyes and azo dyes such as the sorption of direct blue 15 by A. xylinum ATCC 23768 cellulose [121], *Lactobacillus* sp. bacterial consortium immobilized in sodium alginate for Orange 16 dye removal [122], Brilliant Red HE-3B Reactive Dye sorption on the composite of natural polymers and microbial biomass [123] and Congo Red and Methylene Blue sorption by Streptomyces fradiae [46]. A bacterial surface is generally composed of several potential sorption layers rather than a monolayer and at high concentrations of adsorbate, the adsorbent's surface can be covered by more than one layer of adsorbate, and physisorption often occurs as a multilayer. However, each layer can have a combination of chemisorption and physisorption although any layers that are adsorbed after the first are physically adsorbed. Collectively speaking, physisorption will be the more dominant process occurring on a heterogenous surface of bacteria [124]. In contrast to the result in this study, the adsorption of TB dye onto LS and ZnNPs-LS is endothermic [82] while thermodynamics study in other TB adsorbent works is absent.

7. FTIR Analysis

FTIR analysis makes it possible to validate the biosorption process by identifying the adsorption binding site by observing changes in the functional group [125]. Low transmittance values imply a higher number of bonds in the sample that absorbs light, while high transmittance values suggest the existence of fewer bonds that have vibrational frequencies that correspond to the incoming light. Active functional groups such as amino, hydroxyl, sulphonate, carboxyl, and carbonyl are responsible for the characteristics of binding sites and the attachment of dyes to the surface of proteins [79].

Bacterial biomass comprises polysaccharides, proteins, nucleic acids, lipids, and humic compounds, which are the most abundant chemical constituents. They created various functional groups, including carboxyl, hydroxyl, and amino, that were available on the surface site and capable of attaching the sorbate ion and molecules to the surface [126]. The presence of different functional groups on the surface of the bacterial biomass has been detected using FTIR. Fig. 10 shows several notable peaks in the 4,000-400 cm^{-1} wavenumber region for TB dye. All of the peaks in the area of the current peak were separated into two sections: one for identifying the existence of an active group (1,500 cm^{-1} to 4,000 cm^{-1}) and another for fingerprinting the molecule, which includes peaks less than 1,500 cm^{-1}. The fingerprint print area serves as the molecule's

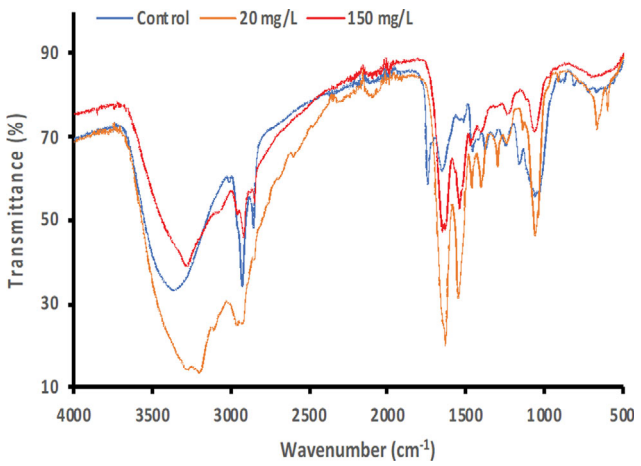

Fig. 10. Comparison of FTIR spectrum of *Pseudomonas* sp. strain MM02 biomass, before and after treatment with 20 and 150 mg/L TB dye.

Table 15. FTIR spectral characteristics of *Pseudomonas* sp. strain MM02 biomass before and after adsorption of TB dye

FTIR peaks	Biomass	20 mg/L	150 ml/L	Action
1	3,365.53	3,274.94	3,282.76	O-H Stretching
2	2,926.29	2,957.66	2,919.38	C-H aliphatic vibration
3	2,855.10	-	2,850.34	C-H (alkyl, alkane)
4	2,168.88	-	-	NH3
5	2,115.58	-	2,096.59	
6	2,036.36	2,089.58	2,015.82	
7	1,998.99	-	1,990.05	
8	1,744.67			C=O stretching (carboxyl)
9	1,652.35		1,652.25	N=N (carboxylic and lactoic)
10	-	1,634.56	1,634.75	Additional peak
11	-	1,549.07	1,539.82	Additional peak
12	1,456.85	1,462.67	1,471.26	N-O
13	-	1,403.32	1,403.85	Additional peak
14	1,377.33			C-C stretching (aromatic ring)
15	1,244.31	1,297.02	1,235.36	S=O: C-O
16	1,161.80	-	-	S=O stretching
17	1,059.30	1,059.00	1,062.31	C-O stretching (ethers or lactones)
18	667.51	664.38	699.02	C-C

unique identifier [126]. More so, Fig. 10 shows a comparison of the FTIR spectrum of *Pseudomonas* sp. strain MM02 biomass before and after treatment with a 20 and 150 mg/L of TB dye.

Table 15 presents a comparison of functional group peaks that were present before and after TB dye adsorption. The FTIR analysis of raw bacterial biosorbent revealed many essential bands within the wavenumber range of 4,000 to 500 cm^{-1}. For example, the absorption peak at 3,365.53 cm^{-1} was moved to 3,282.76 cm^{-1}, indicating the participation of O-H stretching vibrations of H-bonded hydroxyl groups in the dye adsorption [127]. The C-H bond aliphatic group (alkane) vibration was seen to move from 2,926.29 cm^{-1} to 2,919.38cm^{-1} due to symmetric or asymmetric stretching of CH_2 [128,129]. Band between 2,855.10 to 2,850.34 cm^{-1} depicts C-H alkyl stretching, suggesting the formation of methyl derivative. The peak at 1,744.67 cm^{-1} represents C=O stretching while a stretching N=N at 1,652.35 cm^{-1} shows the existence of an azo bond in the dye structure, and the peak at 1,456.85 cm^{-1} indicates N-O stretching. The peak at 161.80 cm^{-1} shows the presence of sulfo groups in the products, but reducing their quantity implies that dyes are being deaminated and desulfonated more. The peak at 2,168.88 cm^{-1} is NH_3, suggesting the production of amines. Additional peaks are seen after the adsorption at 1,634.75, 1,539.82, 1,403.85, and 597.85 cm^{-1} showing C-H deformation, which indicates cleavage of the dyes molecule [130,131].

The adsorption and biodegradation of Red M5B by *B. cereus* was discovered by Kadam et al. [132] via a comparison of the FTIR spectra of the control dye and the products generated following full adsorption of the dye. Spectra of the control, Red M5B revealed peaks at 3,430.5, 1,623.8, 1,533.9, 1,393.0, 1,114.8, 1,048.6, 847.4, 753.4, and 619.8 cm^{-1}, which corresponded to N-H stretching, N-N stretching as in azo compounds, N-H deformation, C-N stretching, O-H deformation, C-OH stretching, S-O stretching as in sulfonic acid, C-H stretching and as a result, the difference in spectra between the dye that had not been treated and the dye that had been treated indicated its deterioration. The absence of a peak at 1,623.8 cm^{-1} in the product spectrum demonstrates that the azo bond has been broken, which supports the enzymatic pattern of *B. cereus* as well as the removal of the azo bond during degradation. In another report by Lade et al. [133], the vibrations observed in the FTIR spectra of Trypan Blue dye were at 2,976.08 cm^{-1} (octahedral OC-H stretching), 2,884.66 cm^{-1} (alkanes C-H stretching), 2,359.74 cm^{-1} (amines NH^+ stretching), 1,612.30-1,581.34 cm^{-1} (double azo bond -N=N stretching), 1,492.96 cm^{-1} (nitrosamines N=O stretching), 1,209.38 cm^{-1} (carbonated impurities). It was discovered that after 24 h of treatment with the microbial community, the dye-extracted products had a distinct pattern of absorption peaks. An analysis of the FTIR profiles of dye-decolorized products revealed peaks at 2,883.73 cm^{-1} (alkanes C-H stretching) and 1,677.47 cm^{-1} (nitrites N=O stretching), respectively. There were two peaks of the dye Trypan Blue that were untreated at 1,612.30 and 1,581.34 cm^{-1}. These examples justified the disappearance of many peaks after the adsorption of TB dye by bacterial biomass as seen in Table 15 below.

8. Scanning Electron Microscopy (SEM)

Scanning electron microscopy (SEM) uses a directed beam of electrons to scan the surface of a sample or spacecraft to obtain images [32,134]. When the electrons communicate with atoms in the specimen, they provide different signals that give details about the specimen's surface structure and composition. These techniques and many others, such as AFM (Atomic Force Microscopy), are used to characterize dye biosorption by bacterial biomass [135, 136]. Samples (bacterial biomass) were prepared before and after the batch adsorption experiment [127,137]. The samples were washed, dried, and grounded. The samples were then analyzed using SEM under appropriate resolution (×5,000 magnification) at a given voltage [138]. A previous adsorption study of bacterial biomass by

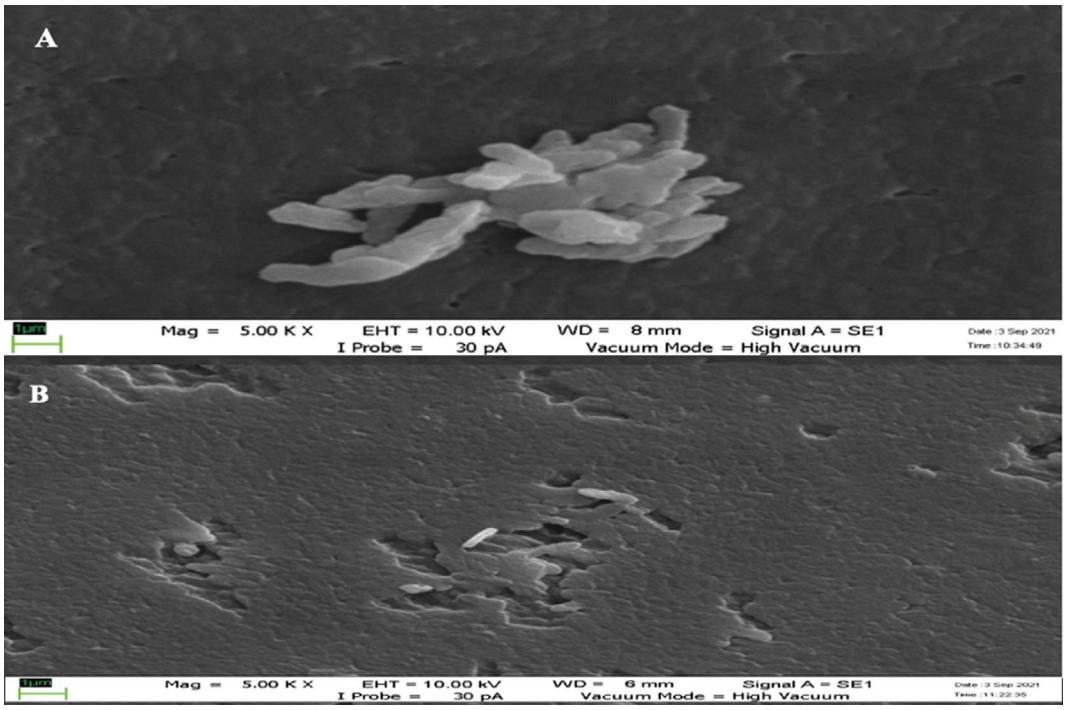

Fig. 11. SEM of *Pseudomonas* sp. strain MM02 biomass, (A) before adsorption, and (B) after TB dye adsorption (Magnification: ×5,000). The scale bar is in green (1 μm).

[136] used scanning electron microscopy (SEM) to examine the surface morphology of the bacterial biomass samples before and after the adsorption. The samples were first dried at 65 °C to a stable weight and then scanned using a scanning electron microscope. From the scanning images, the surface morphology of the biomass was found to be heterogeneous, non-porous, smooth, and tightly packed. The images revealed the presence of adhesive binding on the bacterial biomass surface and that of the dye [139]. Similarly, our work demonstrates that the surface morphology of the *Pseudomonas* sp. strain MM02 biomass is heterogeneous, smooth, and tightly packed. The images (Fig. 11) demonstrated the existence of adhesive binding between the surface of the bacterial biomass and the dye after treatment. Another similar study reported adhesive interactions and the presence of ionized functional groups, phosphodiesters, carboxyl, and amino groups on the surface of Gram-negative cells [136,139]. Additionally, the micrographs demonstrate a distinct variation in the surface appearance of the raw and treated bacterial biomass.

CONCLUSION

This work presents the effective adsorption of TB dye by *Pseudomonas* sp. strain MM02 bacterial biomass previously isolated from the Juru riverine area of Malaysia. The study optimized the adsorption of Trypan Blue (TB) dye in an aqueous solution using screened bacterial biomass. The batch adsorption studies determined the optimum operating parameters for TB dye adsorption. Statistical optimization using RSM resulted in increased adsorption performance of the dye up to 61.51% (59.28% for OFAT), which was validated by the experiment. The adsorption of TB dye by *Pseudomonas* sp. strain MM02 was further characterized for kinetics, isotherms, and thermodynamics. The FTIR results indicate a multi-interaction process between the dye and the surface of the bacteria, with functional groups involved in the interaction, which reflects the complex surface groups occurring on bacterial surfaces in general. Despite this, it is important to note that FTIR is a bulk method, and further surface characterization methods such as X-ray photoelectron spectrometry (XPS), time-of-flight surface ionization mass spectrometry (ToF-SIMS) and contact angle measurements are probably needed to better understand the sorption processes occurring on the surface of the bacteria. The thermodynamic parameters indicate that adsorption conforms to a heterogeneous surface with multilayers, which is typical for bacterial-based biosorbents. The relatively good maximum sorption capacity of the dye to *Pseudomonas* sp. strain MM02 means that the bacterium can be extensively used in the remediation of this dye pollution via adsorption. Our current work includes immobilization processes as a prerequisite for column separation work.

DECLARATIONS

Availability of Data and Materials

Data availability request, the corresponding author will provide any of the data, models, or programs developed or utilized during the study.

Competing Interests

All authors of the manuscript have read and agreed to its content and are accountable for all aspects of the accuracy and integrity of the manuscript in accordance with COPE criteria.

Funding

This research is funded under the Fundamental Research Grant Scheme (FRGS/1/2019/STG05/UPM/02/7) by the Ministry of Higher Education (MOHE) Malaysia.

Authors' Contributions

The experiment was carried out by the first author, Abubakar Abdussamad, who also authored a draft of the paper. Motharasan Manogaran did the isothermal and kinetics modelling statistics. Ahmad Razi Othman, Nur Adeela Yasid, and the corresponding author Yunus Shukor edited the paper and offered recommendations for improvement.

REFERENCES

1. N. Jayanth, R. Karthik, S. Logesh and S. R. K, K. Vijayanand, *Int. Proc. Chem. Biol. Environ. Eng. IPCBEE*, **4**, 120 (2011).
2. M. B. Kurade, M. K. Awasthi, S. P. Govindwar, B. H. Jeon and D. Kalyani, *Front. Microbiol.*, **12**, 10 (2021).
3. K. P. Singh, S. Gupta, A. K. Singh and S. Sinha, *J. Hazard. Mater.*, **186**, 1462 (2011).
4. R. B. Chavan, *Indian J. Fibre Text. Res.*, **26**, 11 (2001).
5. S. D. Kalme, G. K. Parshetti, S. U. Jadhav and S. P. Govindwar, *Bioresour. Technol.*, **98**, 1405 (2007).
6. P. Kumar, H. Bhati, A. Rani and R. Singh, *Life Sci.*, **4**, 38 (2015).
7. S. Mohan, N. Muralimohan, K. Vidhya and C. T. Sivakumar, *Indian J. Sci. Res.*, **17**, 80 (2017).
8. M. M. Islam, K. Mahmud, O. Faruk and S. Billah, *Proc. Int. Conf. Green Technol. Environ. Conserv. GTEC-2011*, **2**, 173 (2011).
9. M. Izuan, E. Halmi, B. Gunasekaran, A. Razi Othman and F. A. Dahalan, *Bioremed. Sci. Technol. Res.*, **3**, 7 (2015).
10. M. Manogaran, N. A. Yasid, A. R. Othman, B. Gunase-karan, M. I. E. Halmi and M. Y. A. Shukor, *Int. J. Environ. Res. Public Health*, **18**, 2424 (2021).
11. B. Lellis, C. Z. Fávaro-polonio, J. A. Pamphile and J. C. Polonio, *Biotechnol. Res. Innov.*, **3**, 275 (2019).
12. N. Puvaneswari, J. Muthukrishnan and P. Gunasekaran, *Indian J. Exp. Biol.*, **44**, 618 (2006).
13. M. E. Karim, K. Dhar and M. T. Hossain, *J. Genet. Eng. Biotechnol.*, **16**, 375 (2018).
14. Z. M. Şenol, *Int. J. Environ. Anal. Chem.*, **16**, 1 (2020).
15. G. M. Walker and L. R. Weatherley, *Environ. Pollut.*, **99**, 219 (2000).
16. T. T. El-Idreesy, O. Khoshala, A. Firouzi and H. A. Elazab, *Biointerface Res. Appl. Chem.*, **11**, 11042 (2021).
17. K. Vijayaraghavan and Y. S. Yun, *Biotechnol. Adv.*, **26**, 266 (2008).
18. Y. Wang, L. Jiang, H. Shang, Q. Li and W. Zhou, *Environ. Technol. Innov.*, **19**, 100810 (2020).
19. N. Kamairudin, S. S. Hoong, L. C. Abdullah, H. Ariffin and D. R. A. Biak, *Molecules*, **26**, 648 (2021).
20. G. Baskar, C. Sriharini, R. Sripriya and S. K. Pavithra, *Int. J. Environ. Sustain. Dev.*, **15**, 241 (2016).
21. M. Ismail, K. Akhtar, M. I. Khan, T. Kamal, M. A. Khan, A. M. Asiri, J. Seo and S. B. Khan, *Curr. Pharm. Des.*, **25**, 3645 (2019).
22. O. Abdi and M. Kazemi, *J. Mater. Environ. Sci.*, **6**, 1386 (2015).
23. G. Crini and E. Lichtfouse, *Green adsorbents for pollutant removal: Fundamentals and design*, Cham, Switzerland (2018).
24. S. Hussain, Z. Maqbool, S. Ali, T. Yasmeen, M. Imran, F. Mahmood and F. Abbas, *Ecotoxicol. Environ. Saf.*, **98**, 331 (2013).
25. V. Karthik, K. Saravanan, N. Sivarajasekar and N. Suriyanarayanan, *Ecol. Environ. Conserv.*, **22**, S423 (2016).
26. D. Park, Y. S. Yun and J. M. Park, *Biotechnol. Bioprocess Eng.*, **15**, 86 (2010).
27. S. W. Won, M. H. Han and Y. Yun, *Water Res.*, **42**, 4847 (2008).
28. F. El-Mched, Z. Olama and H. Holail, *Basic Res. J. Microbiol.*, **1**, 17 (2013).
29. H. P. J. S. Pillai, *J. Pure Appl. Microbiol.*, **11**, 1757 (2017).
30. J. N. Sahu, J. Acharya and B. C. Meikap, *J. Hazard. Mater.*, **172**, 818 (2009).
31. A. Das and S. Mishra, *J. Environ. Chem. Eng.*, **5**, 612 (2017).
32. Y. Gopalakrishnan, A. Al-Gheethi, M. A. Malek, M. M. Azlan, M. Al-Sahari, R. M. S. Radin Mohamed, S. Alkhadher and E. Noman, *Sustainability*, **12**, 1 (2020).
33. Z. Alam, S. A. Muyibi and J. Toramae, *J. Environ. Sci.*, **19**, 674 (2007).
34. M. A. Zahed, H. A. Aziz, L. Mohajeri, S. Mohajeri, S. R. M. Kutty and M. H. Isa, *J. Hazard. Mater.*, **184**, 350 (2010).
35. N. N. A. Razak and M. S. M. Annuar, *Appl. Biochem Biotechnol.*, **172**, 2932 (2014).
36. H. Lade, A. Kadam, D. Paul and S. Govindwar, *Int. J. Environ. Res. Public. Health*, **12**, 3480 (2015).
37. J. Brierley, C. Brierley and G. M. Goyak, *Proceedings of the Sixth International Symposium on Biohydrometallurgy*, Vancouver, B.C., Canada, August 21-24 (1986).
38. S. K. Das, I. Shome and A. K. Guha, *Sep. Sci. Technol.*, **47**, 193 (2012).
39. B. V. Canizo, E. Agostini, A. L. W. Oller, G. L. Dotto, I. A. Vega and L. B. Escudero, *Water Air, Soil Pollut.*, **230**, 1 (2019).
40. F. Huang, Z. Dang, C. L. Guo, G. N. Lu, R. R. Gu, H. J. Liu and H. Zhang, *Colloids Surf. B Biointerfaces*, **107**, 11 (2013).
41. C. Liu, H. Yuan, J. Yang and B. Li, *Afr. J. Biotechnol.*, **10**, 16626 (2011).
42. Z. Cheng, K. Feng, Y. Su, J. Ye, D. Chen, S. Zhang, X. Zhang and D. D. Dionysiou, *Bioresour. Technol.*, **300**, 122705 (2020).
43. M. Manogaran, B. Manogaran, A. R. Othman, B. Gunasekaran and B. M. Y. Abd Shukor, *Bioremed. Sci. Technol. Res.*, **8**, 23 (2020).
44. A. Moussa, C. Abdelhamid, K. Samia, A. Tounsia and T. Mohamed, *J. Environ. Anal. Toxicol.*, **57**, 1 (2015).
45. V. Rizzi, A. Longo, P. Fini, P. Semeraro, P. Cosma, E. Franco, R. García, M. Ferrándiz, E. Núñez, J. A. Gabaldón, I. Fortea, E. Pérez and M. Ferrándiz, *Adv. Chem. Eng. Sci.*, **04**, 454 (2014).
46. Z. Velkova, G. Kirova, M. Stoytcheva and V. Gochev, *J. Serbian Chem. Soc.*, **83**, 107 (2018).
47. Y. Hamzeh, A. Ashori, E. Azadeh and A. Abdulkhani, *Mater. Sci. Eng. C*, **32**, 1394 (2012).
48. S. Busi, R. Chatterjee, J. JRajikumari and S. Hnamte, *J. Environ. Biol.*, **37**, 267 (2015).
49. M. I. Abdullah, A. Öztürk and E. Bayol, *Environ. Earth Sci.*, **80**, 1 (2021).
50. K. M. Sarim, K. Kukreja, I. Shah and C. K. Choudhary, *Bioremed. J.*, **23**, 185 (2019).
51. C. K. Lim, H. H. Bay, A. Aris and Z. Abdul, *Environ. Sci. Pollut. Res.*, **20**, 5056 (2013).
52. Z. D. Umar, A. A. Nor Azwady, S. Z. Zulkifli and M. Muskhazli, *Egypt. J. Pet.*, **27**, 349 (2018).
53. U. Roy, S. Manna, S. Sengupta, P. Das, S. Datta, A. Mukhopadhyay

and A. Bhowal, *Green Adsorbents Pollut. Remov. Environ. Chem. Sustain. World*, **19**, 253 (2018).
54. S. Lagergren and K. Sven. *Vetenskapsakademiens Handl.*, **24**, 1 (1898).
55. G. McKay, Y. S. Ho and J. C. Y. Ng, *Sep. Purif. Methods*, **28**, 87 (1999).
56. G. Blanchard, M. Maunaye and G. Martin, *Water Res.*, **18**, 1501 (1984).
57. F. W. Cope, *Bull. Math. Biophys.*, **34**, 419 (1972).
58. H. N. Tran, S.-J. You and H.-P. Chao, *J. Environ. Chem. Eng.*, **4**, 2671 (2016).
59. E. C. Lima, A. A. Gomes and H. N. Tran, *J. Mol. Liq.*, **311**, 113315 (2020).
60. H. J. Motulsky and L. A. Ransnas, *FASEB J. Off. Publ. Fed. Am. Soc. Exp. Biol.*, **1**, 365 (1987).
61. G. M. Ratnamala and K. Brajesh, *Int. J. Sci. Environ. Technol.*, **2**, 80 (2013).
62. G. Crini and P. M. Badot, *Prog. Polym. Sci.*, **33**, 399 (2008).
63. F. Chen, P. Fang, Y. Gao, Z. Liu, Y. Liu and Y. Dai, *Chem. Eng. J.*, **204**, 107 (2012).
64. S. B. Jadhav, S. M. Yedurkar, S. S. Phugare and J. P. Jadhav, *Clean - Soil Air Water*, **40**, 551 (2012).
65. A. A. L. de Silva, M. A. R. de Carvalho, S. A. L. de Souza, P. M. T. Dias, R. G. da Silva Filho, C. S. de Meirelles Saramago, C. A. de Melo Bento and E. Hofer, *Braz. J. Microbiol. Publ. Braz. Soc. Microbiol.*, **43**, 1620 (2012).
66. R. M. Karakagh, M. Chorom, H. Motamedi, Y. K. Kalkhajeh and S. Oustan, *Ecohydrol. Hydrobiol.*, **12**, 191 (2012).
67. Y. Liu and J. Wang, *Fundamentals and applications of biosorption*, Nova Science Publishers (2009).
68. K. A. Shroff and V. K. Vaidya, *Chem. Eng. J.*, **171**, 1234 (2011).
69. U. V. Mane, P. N. Gurav, A. M. Deshmukh and S. P. Govindwar, *Malay. J. Microbiol.*, **4**, 1 (2008).
70. P. Ramalingam and S. V. Devi, *Int. J. Bio-Technol. Res. IJBTR*, **7**, 1 (2017).
71. R. K. Sheshdeh, M. R. K. Nikou, K. Badii, N. Y. Limaee and G. Golkarnarenji, *J. Taiwan Inst. Chem. Eng.*, **45**, 1792 (2014).
72. J. Nath and L. Ray, *Biochem. Pharmacol.*, **3**, 386 (2015).
73. A. Salihu, M. Bala and S. M. Bala, *ISRN Biotechnol.*, **2013**, 1 (2013).
74. V. B. Borugadda and V. V. Goud, *Energy Sci. Eng.*, **3**, 371 (2015).
75. M. Manogaran, N. Adeela Yasid and S. Aqlima Ahmad, *J. Environ. Microbiol. Toxicol.*, **6**, 18 (2018).
76. K. Yetilmezsoy, S. Demirel and R. J. Vanderbei, *J. Hazard. Mater.*, **171**, 551 (2009).
77. S. A. Hassanzadeh-Tabrizi and E. Taheri-Nassaj, *J. Sol-Gel Sci. Technol.*, **57**, 212 (2011).
78. S. Ibrahim and K. N. M. Zahri, P. Convey, K. A. Khalil, C. Gomez-Fuentes, A. Zulkarnain, S. A. Alias, G. González-Rocha and S. A. Ahmad, *Electron. J. Biotechnol.*, **48**, 1 (2020).
79. S. B. Jadhav, S. N. Surwase, S. S. Phugare and J. P. Jadhav, *Int. J. Environ. Sci. Technol.*, **10**, 181 (2013).
80. K. Y. Foo and B. H. Hameed, *Chem. Eng. J.*, **187**, 53 (2012).
81. N. O. Eddy, R. Garg, R. Garg, A. O. Aikoye and B. I. Ita, *Biomass Conv. Bioref.*, 1 (2022).
82. H. Nadaroglu, S. Cicek and A. A. Gungor. *Spectrochim. Acta - Part Mol. Biomol. Spectrosc.*, **172**, 2 (2017).
83. M. Eid, P. Zhou, X. Wei, J. Zhu, T. Ai, D. Wu, F. Geng, H. Liang, J. Li and B. Li, *J. Mol. Liq.*, **328**, 115401 (2021).
84. H. Freundlich, *Z. Phys. Chem.*, **57**, 385 (1907).
85. G. Rushton, C. Karns and K. Shimizu, *Anal. Chim. Acta*, **528**, 107 (2005).
86. Q. Hu, S. Pang and D. Wang, *Sep. Purif. Rev.*, **125**, 8494 (2021).
87. S. Sadhasivam, E. Saritha, S. Savitha and K. Swaminathan, *Bull. Environ. Contam. Toxicol.*, **75**, 1046 (2005).
88. B. H. Hameed and M. I. El-Khaiary, *J. Hazard. Mater.*, **154**, 639 (2008).
89. I. Langmuir, *J. Am. Chem. Soc.*, **38**, 2221 (1916).
90. K. Y. Foo and B. H. Hameed, *Chem. Eng. J.*, **156**, 2 (2010).
91. T. W. Weber and R. K. Chakravorti, *AIChE J.*, **20**, 228 (1974).
92. K. S. Walton and R. Q. Snurr, *J. Am. Chem. Soc.*, **129**, 8552 (2007).
93. N. Sivarajasekar and R. Baskar, *Desalination Water Treat.*, **52**, 7743 (2014).
94. S. Ahmed, Y. Guo, D. Li, P. Tang and Y. Feng, *Environ. Sci. Pollut. Res.*, **25**, 24907 (2018).
95. D. S. Jovanović, *Kolloid-Z. Amp Z. Für Polym.*, **235**, 1203 (1969).
96. O. Redlich and D. L. Peterson, *J. Phys. Chem.*, **63**, 1024 (1959).
97. N. Ayawei, A. N. Ebelegi and D. Wankasi, *J. Chem.*, **2017**, e3039817 (2017).
98. Y. C. Wong, Y. S. Szeto, A. Cheung and G. Mckay, *Process Biochem.*, **39**, 695 (2004).
99. J. Toth, *Acta Chim. Acad. Sci. Hung.*, **69**, 311 (1971).
100. K. V. Kumar, S. Gadipelli, C. A. Howard, W. Kwapinski and D. J. L. Brett, *J. Mater. Chem. A*, **9**, 944 (2021).
102. D. Do, *Adsorption analysis: Equilibria and kinetics*, Imperial College Press, London (1998).
103. Z. Saadi, R. Saadi and R. Fazaeli, *J. Nanostructure Chem.*, **3**, 48 (2013).
104. A. B. Pérez-Marín, V. M. Zapata, J. F. Ortuño, M. Aguilar, J. Sáez and M. Lloréns, *J. Hazard. Mater.*, **139**, 122 (2007).
105. Y. Torkia and M. Khalfaoui, *IOSR J. Appl. Phys.*, **6**, 62 (2014).
106. M. I. Temkin and V. Pyzhev, *Acta Physicochim USSR*, **12**, 327 (1940).
107. K. H. Chu, *Ind. Eng. Chem. Res.*, **60**, 13140 (2021).
108. A. R. Khan, R. Ataullah and A. Al-Haddad, *J. Colloid Interface Sci.*, **194**, 154 (1997).
109. S. Brunauer, P. H. Emmett and E. Teller, *J. Am. Chem. Soc.*, **60**, 309 (1938).
110. A. Ebadi, J. S. Soltan Mohammadzadeh and A. Khudiev, *Adsorption*, **15**, 65 (2009).
111. W. R. Vieth and K. J. Sladek, *J. Colloid Sci.*, **20**, 1014 (1965).
112. B. Balci and F. E. Erkurt, *Adsorpt. Sci. Technol.*, **35**, 339 (2017).
113. W. Fritz and E.-U. Schluender, *Chem. Eng. Sci.*, **29**, 1279 (1974).
114. A. Benmessaoud, N. Djamel, E. H. Mekatel and A. Samira, *Iran. J. Chem. Chem. Eng.-Int. Engl. Ed.*, **39**, 153 (2020).
115. D. P. Valenzuela and A. L. Myers, *Adsorption equilibrium data handbook*, Prentice Hall, Englewood Cliffs, N.J. (1989).
116. G. McKay, A. Mesdaghinia, S. Nasseri, M. Hadi and M. Solaimany Aminabad, *Chem. Eng. J.*, **251**, 236 (2014).
117. A. W. Marczewski, *Appl. Surf. Sci.*, **256**, 5145 (2010).
118. V. J. Inglezakis and S. Poulopoulos, *Adsorption, ion exchange and catalysis: Design of operations and environmental applications*, 1st ed., Elsevier (2006).
119. P. Saha and S. Chowdhury, *Thermodynamics*, **16**, 349 (2011).
120. C. G. Hill and T. W. Root, *Introduction to chemical engineering*

kinetics and reactor design, 2nd ed., Wiley, New York, NY (1977).
121. A. Ashjaran, M. E. Yazdanshenas, A. Rashidi, R. Khajavia and A. Rezaee, *Afr. J. Microbiol. Res*., **6**, 1270 (2012).
122. D. Şuteu, C. Zaharia, A. C. Blaga and A. C. Peptu, *Desalination Water Treat*., **246**, 315 (2022).
123. D. Suteu, A. C. Blaga, R. Cimpoesu, A. C. Puițel and R.-E. Tataru-Farmus, *Polymers*, **13**, 4314 (2021).
124. M. Tatianna, L. Kristine, G. M. Alejandro, L. Loong, Tak, W. Xiuju and P. Erica, *SN Appl. Sci*., **3**, 1 (2021).
125. L. N. Du, B. Wang, G. Li, S. Wang, D. E. Crowley and Y. H. Zhao, *J. Hazard. Mater*., **205-206**, 47 (2012).
126. J. Gupta, R. Rathour, K. Medhi, B. Tyagi and I. S. Thakur, *Microbial-derived natural bioproducts for a sustainable environment: A bioprospective for waste to wealth*, Elsevier Inc. (2019).
127. M. Fawzy, M. Nasr, A. M. Abdel-Rahman, G. Hosny and B. R. Odhafa, *Int. J. Phytoremediation*, **21**, 1205 (2019).
128. D. C. Kalyani, A. A. Telke, R. S. Dhanve and J. P. Jadhav, *J. Hazard. Mater*., **163**, 735 (2009).
129. M. Thanavel, S. K. Kadam, S. P. Biradar, S. P. Govindwar, B. H. Jeon and S. K. Sadasivam, *SN Appl. Sci*., **1**, 1 (2019).
130. M. A. Ahmad Farid, M. A. Hassan, A. M. Roslan, H. Ariffin, M. N. F. Norrrahim, M. R. Othman and S. Yoshihito, *Environ. Sci. Pollut. Res*., **28**, 27976 (2021).
131. R. V. Khandare, A. N. Kabra, A. V. Awate and S. P. Govindwar, *Int. J. Environ. Sci. Technol*., **10**, 1039 (2013).
132. A. A. Kadam, J. D. Kamatkar, R. V. Khandare, J. P. Jadhav and S. P. Govindwar, *Environ. Sci. Pollut. Res*., **20**, 1009 (2013).
133. H. Lade, A. Kadam, D. Paul and S. Govindwar, *Int. J. Environ. Res. Public Health*, **12**, 3480 (2015).
134. Z. Chen, H. Chen, X. Pan and Z. Lin, *Water. Air. Soil Pollut*., **226**, 1 (2015).
135. P. Kotrba, M. Mackova and T. Macek, *Microb. Biosorption Met*., 1 (2011).
136. T. Anh, C. Fu and R. Juang, *J. Environ. Manage*., **182**, 265 (2016).
137. J. Gao, J. Ye, J. Ma, L. Tang and J. Huang, *J. Hazard. Mater*., **276**, 112 (2014).
138. S. Venkata Mohan, N. Chandrasekhar Rao and J. Karthikeyan, *J. Hazard. Mater*., **90**, 189 (2002).
139. D. T. Nguyen, H. N. Tran, R. S. Juang, N. D. Dat, F. Tomul, A. Ivanets, S. H. Woo, A. Hosseini-Bandegharaei, V. P. Nguyen and H. P. Chao, *J. Environ. Chem. Eng*., **8**, 104408 (2020).
140. A. Öztürk, E. Bayol and M. I. Abdullah, *Electron. J. Biotechnol*., **46**, 22 (2020).
141. S. Mona, A. Kaushik and C. P. Kaushik, *Ecol. Eng*., **37**, 1589 (2011).
142. F. Colak, N. Atar and A. Olgun, *Chem. Eng. J*., **150**, 122 (2009).